University of Tasmania

Doctoral Thesis

A Kinematical Approach to Gravitational Lensing

Author:
Stephen Walters

Supervisors:
Dr. Larry Forbes
Dr. Andrew Cole
Dr. Peter Jarvis

A thesis submitted in fulfilment of the requirements for the degree of Doctor of Philosophy

in the

School of Mathematics and Physics

October 2014

Declaration of Authorship

I, Stephen Walters, declare that this thesis titled, 'A Kinematical Approach to Gravitational Lensing' and the work presented in it are my own. I confirm that:

- This work was done wholly while in candidature for a research degree at this University.
- This thesis contains no material which has been accepted for a degree or diploma by the University or any other institution, except by way of background information and duly acknowledged in the thesis, and to the best of my knowledge and belief no material previously published or written by another person except where due acknowledgement is made in the text of the thesis, nor does the thesis contain any material that infringes copyright.
- Where I have consulted the published work of others, this is always clearly attributed.
- Where I have quoted from the work of others, the source is always given. With the exception of such quotations, this thesis is entirely my own work.
- I have acknowledged all main sources of help.
- Where the thesis is based on work done by myself jointly with others, I have made clear exactly what was done by others and what I have contributed myself.

Signed: _____

Date: _____

Statement of Co-Authorship

The following three articles form the majority of the content of this thesis. Estimated contributions from authors are given.

A kinematical approach to gravitational lensing using new formulae for refractive index and acceleration
Walters, Forbes & Jarvis (2010)
Steve Walters 70%, Larry Forbes 20%, Peter Jarvis 10%

A note on a linearized approach to gravitational lensing
Walters & Forbes (2011)
Steve Walters 80%, Larry Forbes 20%

Rotating gravitational lenses: a kinematic approach
Walters & Forbes (2014) (submitted)
Steve Walters 80%, Larry Forbes 20%

I agree with the estimated contributions for each of the published or submitted peer-reviewed papers mentioned above:

Signed: _____

Date: _____

Dr Larry Forbes
Supervisor
School of Mathematics and Physics
University of Tasmania

Authority of Access

Abstract

The deflection of light by massive bodies has been of interest to mathematicians and physicists from time to time since Newton suggested the possibility in his 1704 work, "Opticks". This deflection was calculated in the late eighteenth and early nineteenth centuries, treating light as a classical particle. The deflection was again calculated by Einstein in the early twentieth century, using his new general theory of relativity, to be twice the previous classical result. The measurement of the deflection of light passing close by the Sun was widely publicized as a dramatic confirmation of general relativity, in the now famous 1919 expeditions.

In the last three decades, gravitational lensing has become an important tool for astrophysicists, especially in searching for dark matter and exoplanets. By 1991, astrophysicists were suggesting that exoplanets could be found using microlensing, and since 2004 at least ten planets have been found in this way. In microlensing, light from a background star passes close to the lensing system, and is deflected around the lens. Because of this, more light rays reach the observer, producing magnification of the background source. This magnification changes over time, as the source, lens and observer move into and out of alignment. The details of the magnification over time are plotted in a 'light curve', which is simply intensity versus time. A planet orbiting a lensing star can make changes in the light field at the observer's plane ("magnification map"). Such changes show up as variations to the shape of the simple light curve.

This thesis presents a mathematical model for the paths taken by light rays near a massive object such as a star or black hole. I begin the thesis by considering the spacetime around a non-rotating, uncharged, spherically symmetric object. Such a spacetime is described by the Schwarzschild metric equation. After considering the deflection angle and travel-time delay in such a system, I derive an acceleration vector for the massless particle ("photon"). This acceleration vector is used to plot the light paths of many photons passing through a binary system using numerical integration, resulting in a magnification map very similar to those currently in use by astrophysicists. In the following chapter I consider a linear approximation of the acceleration vector just mentioned, considering the light path as a small perturbation about a straight line. Such an approach results in a linear third order ordinary differential equation, but with non-constant coefficients. Unexpectedly, a closed-form solution is found, resulting in path equations accurate to first order in the relevant small parameter. This allows for very rapid computation of the magnification map. Some examples are presented and compared against the fully non-linear numerical results of the previous chapter, and also against a simpler approach used by some other authors.

The final section of results of the thesis is given to consideration of the effect of rotation of the lensing object. In considering the Kerr metric which describes such a system, I follow an approach similar to that used in previous chapters. Thus, an acceleration vector is derived, which is used to plot a magnification map for a binary system containing a rotating object. Rotation causes bending and asymmetry in the magnification map. This is illustrated for certain cases of interest. A second order approximation is also considered, as well as application of the equatorial special case to calculation of travel time delay. This delay is compared to that expected for a non-rotating object.

Acknowledgements

I wish to express my heartfelt thanks to my primary supervisor, Dr Larry Forbes, for your patient and kind support from beginning to end of this work. Your mathematical insight, combined with timely advice, and encouragement, not to mention the numerous cups of coffee, have been invaluable to me in bringing this research to fruition. Thank you.

I also would like to thank Dr Andrew Cole and Dr Peter Jarvis for encouragement and helpful comments, especially regarding aspects of relativity theory and astrophysics.

Finally, I would like to acknowledge the generous financial support afforded me through a Tasmanian Research Scholarship and an Australian Postgraduate Award in the course of this research.

Contents

List of Figures

List of Tables

Chapter 1

Introduction

1.1 Historical Background

The deflection of light by massive bodies has been of interest to mathematicians and physicists since Newton suggested the possibility in the form of a question for further study in Book 3 of his "Opticks". He suggests that like any material object, light too, should be deflected by the gravitational attraction of all other matter. "Do not Bodies act upon Light at a distance, and by their action bend its Rays; and is not this action strongest at the least distance?" (Newton, 1704). This appears to have been a prevailing view in the eighteenth century, as stated by clergyman and scientist, John Michell in his paper (Michell, 1784) on determining the distances to stars as well as their magnitudes.

> *Let us now suppose the particles of light to be attracted in the same manner as all other bodies with which we are acquainted; that is, by forces bearing the same proportion to their vis inertiae, of which there can be no reasonable doubt, gravitation being, as far as we know, or have any reason to believe, an universal law of nature. Upon this supposition then, if any one*

> *of the fixed stars, whose density was known by the above-mentioned means, should be large enough sensibly to affect the velocity of the light issuing from it, we should have the means of knowing its real magnitude, &c.*

Later in the same paper Michell gives a description of an hypothetical star so massive that light would be unable to escape its surface, and which consequently would be invisible to us. This appears to be the first mention of a black hole in the literature. In the same method of reasoning, Johann von Soldner published a paper in 1801, which by careful calculation, determined the deflection of light from a distant star as it passes near to the sun. He thus found the deflection to be 0.84 arcseconds. With the limits of precision of astronomical observations at the time, Soldner concludes "that nothing makes it necessary, at least in the present state of practical astronomy, that one should take into account the perturbation of light rays by attracting celestial bodies" (see the commentary and translation of Soldner's paper by Jaki (1978), as well as the note by Treder & Jackisch (1981), who provide additional clarification).

In the early twentieth century, an approximation of the deflection of light passing close to the sun was again calculated by Einstein, using his new general theory of relativity. This deflection was found to be twice the previous classical result. By this time, astronomical measurement was sufficiently precise to measure such small deflections, and the measurement of the deflection of light passing close by the sun by Eddington and Dyson was widely publicized as a dramatic confirmation of general relativity, in the now famous 1919 expeditions. Einstein considered the "Lens-like action of a star" due to this deflection in a paper in 1936, but concluded by saying that the chance of actually observing the phenomena was exceedingly remote, due to the very close alignment required between source, lens and observer (Einstein, 1936).

In the last three decades, following the discovery of the first known double imaged quasar in 1979, gravitational lensing has become an important tool for astrophysicists. In a paper published in 1986, Paczyński suggested that it may be practical to observe microlensing events produced by dark lenses in the galactic halo, by means of an observing program designed to monitor the brightness of several million stars in neighbouring galaxies over a two year period. At least, such a program would put constraints on the masses of the intervening halo objects (Paczyński, 1986). By 1991, astrophysicists were suggesting that exoplanets could be found using microlensing (Mao & Paczyński, 1991). The first found using this method was discovered in 2003 (Bond et al., 2004) with several more discovered since (Sumi et al., 2010). While far more planets are discovered by other methods such as radial velocity measurement or light dimming due to transiting planets, micro-lensing complements these methods, being more sensitive to planets with larger orbits (Mao, Kerins & Rattenbury, 2007).

1.2 Gravitational Lensing

When light from a background star passes close to a heavy object or distribution of matter, it is deflected towards this 'lens'. Because of this, more light rays reach the observer, producing magnification and distortion of the background source image. A distinction is made between Strong Lensing and Microlensing, in that a Strong Lensing event separates the different images to an observable extent. That is, separate images of the background object can be seen. A typical strong lens would be a cluster of galaxies, lensing a more distant galaxy. Microlensing events produce images that are so close together that they cannot be distinguished, resulting only in an apparent brightening of the background source. Typically, the lens would

be a stellar system, a black hole, or a planet, and the source would be a single star. The approach in this study can be used for either sort of lensing, but most of the discussion will relate to microlensing and the resultant magnification maps and light intensity curves. The magnification thus produced changes over time, as the source, lens and observer move into and out of alignment. The details of the magnification over time are plotted in a 'light curve', which is simply intensity versus time. A planet orbiting a lensing star can make changes in the magnification pattern at the observer's plane. Such changes show up as variations to the shape of the simple light curve.

This phenomenon, known as gravitational lensing, is used by astrophysicists in identifying characteristics of the lensing object. Such an approach is useful in searching for dark matter, as suggested by Paczyński (1986). The presence of such planets in the lensing system can cause caustics in the magnification map. These caustics are described by Gould & Loeb (1992). Various techniques can be used to model caustic patterns.

Interpretation of these light curves is difficult, as this is an inverse problem, in which observers seek to determine the details of the lensing system which gave rise to the observed data. In particular, researchers are often trying to find planets in the lensing system, and to determine characteristics of such planets, primarily orbital radius and mass. Details on reproducing a model of such a multi-body lens were outlined at least as early as 1996 (Wambsganss, 1997). For an introduction including a brief history, background, theory and application of gravitational lensing, the following works are recommended: Schneider, Ehlers & Falco (1992), Mao et al. (2007), or the excellent recent reviews by Gaudi (2012), Bennett (2008), and Ellis (2010).

1.3 Lensing Models

It is customary (Wambsganss, 1997) to use a 'thin lens' model, in which the effect of the lensing system is confined to the plane containing the lensing objects (the 'lens plane'), this plane being normal to the line from source to observer. A deflected light ray thus consists approximately of two straight lines, with an abrupt angle change in the lens plane. The magnitude of this change is given by the Einstein deflection angle: $\Delta\theta = 2r_s/r_0$ where r_0 is the point of closest approach of the light ray to the star or planet and r_s is the Schwarzschild radius, $r_s = 2MG/c^2$. Here, M is the mass of the star, G is Newton's gravitational constant and c is the speed of light in a vacuum. Note that this is sometimes given as $\Delta\theta = 2r_s/b$, where b is the impact parameter. The values of b and r_0 only differ by an amount of the order of the small ratio r_s/r_0, so that to first order in this small parameter, these two estimates are equivalent. For a description of this method, see for example Schneider & Weiss (1986). As the deflection involved is very small (which means that the photon passes through areas of weak gravitational fields only), such a "first order" approach is a very accurate approximation.

Current methods (for example, see Zabel & Peterson (2003) and Wambsganss (1997)) shoot rays from the observer to the lens plane, deflect by the angle as calculated above, and then draw the ray from there to the source plane. Equivalently, light rays may be followed from the source to the observer, mimicking more closely the actual physics. The density of rays at the source plane (or, alternatively, the observer's plane) is thus mapped. By tracing various linear paths across this map, to simulate the relative movement of the source star, light curves are generated. The aim is to find a light curve that is a good fit to the empirical data.

For an observer travelling across the plane normal to the line joining lens and source (the 'observer's plane'), the amplification can be plotted as a function of time. Fig. 1.1 shows schematically the method for mapping the amplification for an observer travelling at constant speed in the observer's plane, not passing through the origin (that is, the intersection of the lens-source line with the observer's plane). Passing through the origin in this point-source-point-lens model (PSPL) would result in an infinite magnification (a more realistic non-point source would not exhibit such pathology, (see Witt & Mao (1994) and as later discussed in Mollerach & Roulet (2002) p.41). The relative intensity I for a PSPL model is given by $I = (u^2 + 2)/(u\sqrt{u^2 + 4})$, where the dimensionless variable u is a measure of the impact parameter (Gould & Loeb (1992) and Wambsganss (1998)). A model light curve generated using this formula is shown in the lower panel of Fig. 1.1. Light curves based on collected intensity data can provide information about the mass of the lensing object, provided that the distance to lens and distance to source can be estimated. If the lens is a binary system, there are deviations from this simple light curve.

The purpose of a microlensing model is to produce a magnification map at the observer's plane due to light from the source (alternatively, a map at the source plane due to light rays from the observer) being deflected at the lens plane. The light curve is then a one dimensional cut through the magnification map. A magnification map such as this can be produced by shooting rays from the source, through the lens and plotting where the ray intersects with the observer's plane, using the deflection angle predicted by general relativity. This approach is shown in the top panel of Fig. 1.1. In reality, the path will be a smooth curve rather than two straight line segments. Even so, the majority of the deflection occurs very close to the lens plane.

FIGURE 1.1: Thin Lens Approach and Typical Light Curve. The top panel is a schematic representation of a point-source-point-lens scenario, showing the path of the observer across an imaginary plane normal to the line through source and lens (the 'observer plane'). The lower panel shows an ideal light curve of I versus t generated by the intensity formula $I = (u^2+2)/(u\sqrt{u^2+4})$, where $u = \sqrt{r_{min} + t^2}$. In this case $r_{min} = 1$. Note that if $r_{min} = 0$, the resultant intensity at $t = 0$ is infinite.

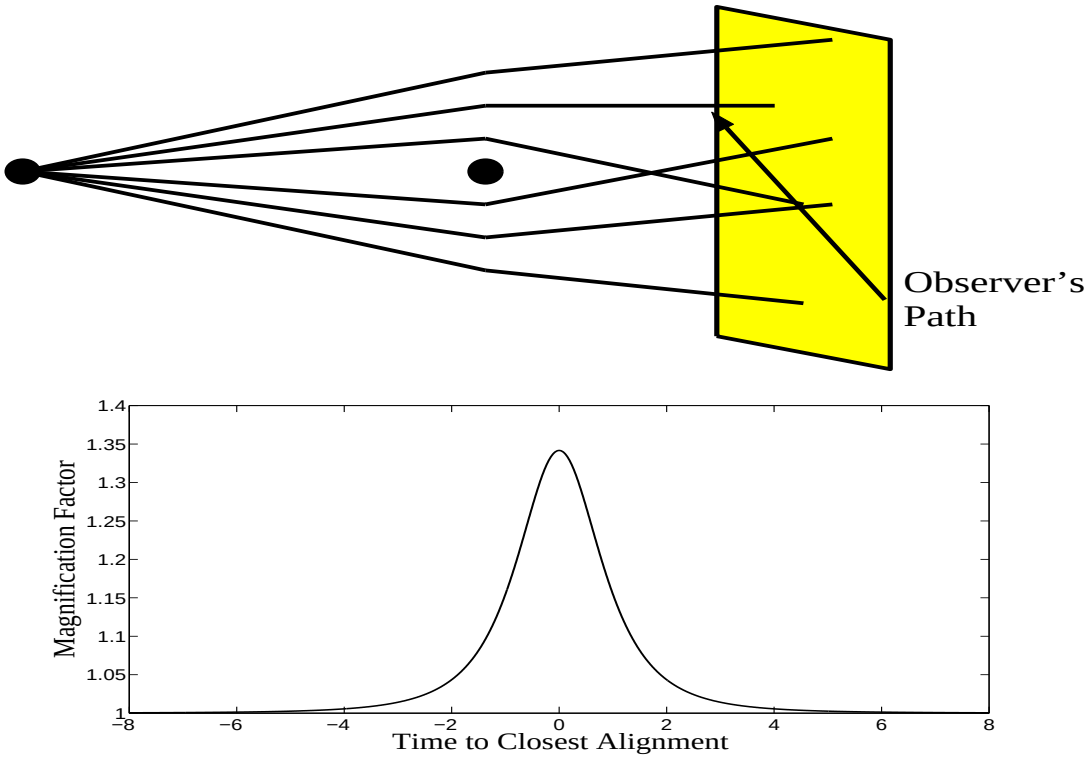

At each small area on the observer's plane, the brightness is proportional to the number of rays passing through that area. A line is then drawn across the observer's plane, representing the passage of the earth relative to lens and source. Along that line, the brightness is sampled and a light curve is the resulting brightness as a function of time for the observer travelling along that line. Note that every such magnification map allows for arbitrarily many light curves, depending on the location of the observer's path across the plane. Because of this, it is, in general, a difficult matter to find a model to fit an observed light curve for a lens

involving more than one mass (that is, a binary or planetary system). The problem becomes much more difficult when the lens involves more than two objects (Mao et al., 2007).

1.4 Kinematical Approach

While Newtonian gravity is a very accurate theory for almost all calculations used in modern life, the deflection of light is an example where it is clearly insufficient. Indeed, as noted above, it predicts a value approximately half of that predicted by general relativity, the relativistic prediction having been confirmed by experiment to high accuracy (Robertson, Carter, & Dillinger, 1991). However, the non-linear equations of General Relativity have not admitted many closed-form solutions, and only a handful of exact solutions are known, for very simple systems with a high degree of symmetry. This has led to several approximations to General Relativity, such as the Weak-Field Approximation and the Post-Newtonian formalism. Additionally, other theories of gravity have been developed which do predict a deflection of light in line with experimental values, and some lensing models have been developed using such theories; for example, see Mortlock &Turner (2001).

It is the purpose of this thesis to consider gravitational lensing using an alternative approach. This approach can be described as an equivalent classical kinematical formulation, which nevertheless replaces Newton's formula for gravitational acceleration with formulae derived from two of the known solutions of general relativity. The first of these is the Schwarzschild metric, which describes space-time around a spherically symmetric uncharged non-rotating mass. The second is the Kerr metric which describes space-time around an uncharged point-mass, rotating or otherwise. An acceleration vector will be developed using these solutions. The

approximation taken for systems consisting of multiple masses will be to calculate the acceleration vector due to each mass and sum these vectors to derive an overall acceleration for the light ray, analogously with Newtonian physics. Using this kinematical approach, each curved light ray is traced from the source to the plane of the observer, rather than using the simple angle change formula commonly used in lensing models. Numerical approaches will be explored, as well as analytical solutions to suitable approximations of the light paths.

This novel approach is intended to be complementary to the thin-lens approach and other methods of analysing gravitational lenses. It will be shown in chapter 4, that this new approach can be useful in easily generating known results for deflection and travel-time delay, as well as in producing at least one new result. As a new tool for such analysis, it is hoped that others will find this approach useful beyond the material in this brief thesis, and will use it to simplify calculations in situations where the kinematical method is more convenient than other approaches.

It has been the author's experience that viewing the predicted effects of a gravitational lens from within different frameworks, such as the thin-lens approach, the kinematical method, and its first order approximation, has been enlightening. As a simple example, the consideration of the distinction between the distance of closest approach, the impact parameter, and the angular momentum term has been clarified by contemplation of these different methods. It is hoped that others will find some such value, pedagogical or otherwise, in this alternative approach.

Chapter 2

Light paths near a non-rotating body

2.1 Introduction

The simplest non-trivial solution to the equations of Einstein's theory of general relativity was discovered by the accomplished German physicist Karl Schwarzschild while serving on the Russian front in 1915. This 'Schwarzschild metric' describes the geometry of space-time in the vacuum surrounding a spherically symmetric, non-rotating, uncharged mass. The kinematic approach of this thesis begins by examining this simplest solution to Einstein's equations. In this chapter the Schwarzschild metric is used to derive an effective refractive index and acceleration vector that account for relativistic deflection of light rays, in an otherwise classical kinematic framework. The new refractive index and the known path equation are integrated to give accurate results for travel time and deflection angle, respectively. A new formula for acceleration is derived which describes the path of a massless

test particle in the vicinity of a spherically symmetric mass density distribution. A standard ray-shooting technique is used to compare the deflection angle and delay time predicted by this new formula with the previously calculated values, and with standard first order approximations. Finally, the ray shooting method is used in theoretical examples of strong and weak lensing, reproducing known observer-plane caustic patterns for multiple masses.

We will start by considering the path predicted by the Schwarzschild metric for a massless test particle ("photon") near a massive body. The changes in angle along this path will be integrated to give the deflection of the light ray predicted by general relativity. As a check, we will compare this result with the known formula for approximating the deflection to first order in the relevant small constant. Next we will derive an 'effective refractive index' due to the massive body. Integration will be used to predict the Shapiro delay, which will also be checked against the known first order prediction of general relativity. A new acceleration formula will then be derived and tested against these known values for the deflection and delay using a forward integration method. Finally, we will describe and exemplify a procedure for using the new acceleration formula to produce magnification maps for multi-body lenses.

2.2 Light Paths in a Schwarzschild System

As stated in Section 2.1 above, the Schwarzschild metric describes spacetime outside a non-rotating, electrically neutral, spherically symmetric mass M and is taken as a valid approximation for local space-time structure in the vicinity of any massive spherical body (stellar systems, including black holes, but also planets) having negligible charge and angular momentum. In spherical coordinates

the metric components are given in terms of the invariant interval dl^2 as (Misner, Thorne & Wheeler, 1973)

$$dl^2 = \frac{r - r_s}{r}c^2dt^2 - \frac{r}{r - r_s}dr^2 - r^2(\sin^2\theta d\phi^2 + d\theta^2), \tag{2.1}$$

where $r_s = 2MG/c^2$ is the Schwarzschild radius, G is Newton's constant, and c is the constant speed of light in vacuum. Here r , θ, ϕ are the Schwarzschild coordinates which correspond to standard spherical coordinates in the reference frame of an observer at rest far from the system.

Light travels on null geodesics with $dl = 0$, so equation (2.1) becomes

$$cdt = \frac{r}{r - r_s}\sqrt{dr^2 + r(r - r_s)(\sin^2\theta d\phi^2 + d\theta^2)}. \tag{2.2}$$

Applying Fermat's principle, that light follows a path that extremizes travel time T, we can consider the functional:

$$T = \int dt = \frac{1}{c}\int \frac{r}{r - r_s}\sqrt{dr^2 + r(r - r_s)(\sin^2\theta d\phi^2 + d\theta^2)}. \tag{2.3}$$

To illustrate the use of equation (2.3) we firstly derive a path equation which is equivalent to the usual trajectory equations for null geodesics, and numerically integrate it to give the deflection of a light ray according to general relativity.

Without loss of generality, for a single light ray, the coordinates can be oriented so that the ray is in the plane $\theta = \pi/2$. Then $d\theta = 0$ in equation (2.3), which consequently may be re-arranged to give

$$T = \frac{1}{c}\int \frac{r}{r - r_s}\sqrt{1 + r(r - r_s)\phi'^2}dr \tag{2.4}$$

adopting the notation $\phi' = d\phi/dr$. Let F be the integrand in equation (2.4), that is:

$$F(r, \phi, \phi') = \frac{r}{r - r_s}\sqrt{1 + r(r - r_s)\phi'^2}. \tag{2.5}$$

Then the Euler-Lagrange equation is

$$\frac{\partial F}{\partial \phi} - \frac{d}{dr}(\frac{\partial F}{\partial \phi'}) = 0. \tag{2.6}$$

It can be seen in equation (2.5), that there is no explicit dependence of F upon ϕ so clearly $\partial F/\partial\phi = 0$. Therefore this term vanishes in equation (2.6) which then has the immediate first integral

$$\frac{\partial F}{\partial \phi'} = \frac{r^2\phi'}{\sqrt{1 + r(r - r_s)\phi'^2}} = K,$$

in which K is a constant. Now $1/\phi' = dr/d\phi$, so rearrangement yields the first order separable ODE

$$\frac{dr}{d\phi} = \pm\sqrt{\frac{r^4}{K^2} - r(r - r_s)}.$$

This constant K can be determined. At the point of closest approach to the mass (call this point $r = r_0$), the radius is at a minimum, that is, $dr/d\phi = 0$, so it follows that:

$$K^2 = \frac{r_0^3}{r_0 - r_s}.$$

Thus the path is defined by:

$$\frac{dr}{d\phi} = \pm\sqrt{\frac{r^4(r_0 - r_s)}{r_0^3} - r(r - r_s)}. \tag{2.7}$$

It can be easily seen that substituting $u = 1/r$ followed by differentiation gives the well known second order equation as (Capozziello et al, 1997)

$$\frac{d^2u}{d\phi^2} + u = \frac{3r_s}{2}u^2. \tag{2.8}$$

From equation (2.7), an integral can easily be written to evaluate the total deflection of light passing a massive object, which will be twice the deflection from the perihelion out to infinity:

$$\triangle\phi = 2\int_{r_0}^{\infty} \frac{dr}{\sqrt{r^4(r_0 - r_s)/r_0^3 - r(r - r_s)}},$$

This elliptic integral cannot be evaluated with a finite number of simple algebraic terms. Numerical integration could be used to evaluate the deflection. However, the integrand is infinite at $r = r_0$, making the accuracy of any numerical evaluation questionable. By using a substitution $r = 1/\cos(2\psi)$, the singularity can be removed. After simplification we obtain:

$$\triangle\phi = 4\sqrt{\frac{2r_0}{r_s}}\int_0^{\pi/4} \frac{d\psi}{\sqrt{2r_0/r_s + 2 - 4\cos^2\psi - \sec^2\psi}}.$$

This integrand is well behaved over the interval, so it can be numerically integrated to any desired accuracy, for example, by Gaussian quadrature. An undeflected ray will have $\triangle\phi = \pi$, so the deflection for a ray will be $\delta = \triangle\phi - \pi$. The deflection is usually very small, so in order to avoid a 'loss of significance error', this subtraction should be performed in the integrand. For readability, let $\alpha = 2r_0/r_s$, and let $\beta = 2 - 4\cos^2\psi - \sec^2\psi$. In this notation, the deflection δ can therefore be expressed as

$$\delta = 4\sqrt{\alpha}\int_0^{\pi/4} (\frac{1}{\sqrt{\alpha + \beta}} - \frac{1}{\sqrt{\alpha}})d\psi.$$

The two terms in the integrand are combined, so that the subtraction can be performed explicitly. This yields:

$$\delta = 4 \int_0^{\pi/4} \left(\frac{-\beta}{\sqrt{\alpha+\beta}(\sqrt{\alpha}+\sqrt{\alpha+\beta})}\right) d\psi. \tag{2.9}$$

For the purposes of this calculation, we take the solar radius to be 696 000 kilometres, and the solar Schwarzschild radius to be 2.95 kilometres. Numerical integration of equation (2.9) for a ray passing near the surface of the sun $(r_s/r_0 = 2.95/696000))$gives a deflection angle of 1.74851634161261 arcseconds. As the path equation contains all of the information about the general relativistic path of the photon, this is the deflection angle predicted by general relativity to the level of precision shown. This deflection angle will be used later to confirm the accuracy of the kinematic approach. As a check, we can consider Einstein's estimate for the deflection angle(Schneider et al. (1992), page 3)

$$\frac{2r_s}{r_0} = 1.74850913341648 \text{ arcseconds.} \tag{2.10}$$

This estimate is found to correspond to our calculated value to first order in r_s/r_0, as expected.

2.3 New Refractive Index & Travel Time Delay

The approach presented here makes use of an expression for the refractive index, n. The Schwarzschild metric from Section 2.2 will be used to derive an 'effective' refractive index. As suggested above, the functional (2.3) can be arranged in the form $T = \int dt = \int (dt/ds)ds$, where s is an arbitrary parametrization of the ray

path. By choosing ds to be the element of arc-length along the path, the speed is then $v = ds/dt$, and thus the refractive index is $n = c/v = cdt/ds$, and we obtain finally $T = 1/c \int nds$, with the refractive index then having the form

$$n = \frac{r}{r - r_s}\sqrt{r'^2 + r(r - r_s)(\sin^2\theta\phi'^2 + \theta'^2)},$$

where $r' = dr/ds$, $\theta' = d\theta/ds$ and $\phi' = d\phi/ds$. (Note that there is no suggestion here of any physical effect on the speed of light - indeed, any local measurement of coordinate velocity is guaranteed to result in the usual speed c).

Taking again the two dimensional (2D) case, with $\theta = \pi/2$, the refractive index has the form

$$n = \frac{r}{r - r_s}\sqrt{r'^2 + r(r - r_s)\phi'^2}. \tag{2.11}$$

As an example, the delay can be calculated for light to travel from an object at earth radius, skim past the sun, and back out to earth radius. This is the calculation needed for the radar echo delay test (the famous "fourth test of relativity" proposed by Shapiro (1964)). (In fact, for that test, it would be necessary to have another satellite (such as Venus or Mars), and the calculation would need to be performed for each leg of the journey. For the purposes of this calculation, it is simpler to imagine a reflecting satellite at the same orbit as the earth). The problem can be pictured as in Fig. 2.1, not to scale. The deflection is small, so that the path appears as a straight line. In fact the curved path that the photon takes is derived above in equation (2.7). The path is symmetric about the point of closest approach (r_0), so that exactly half the delay can be obtained by integrating from r_0 to r_e, the radius of the earth's orbit. If the sun had no effect on the light path, the distance from perihelion to earth would be the straight line distance $\sqrt{r_e^2 - r_0^2}$.

FIGURE 2.1: Photon path near the sun. The distance to perihelion is designated r_0, and r_e is the distance to the earth.

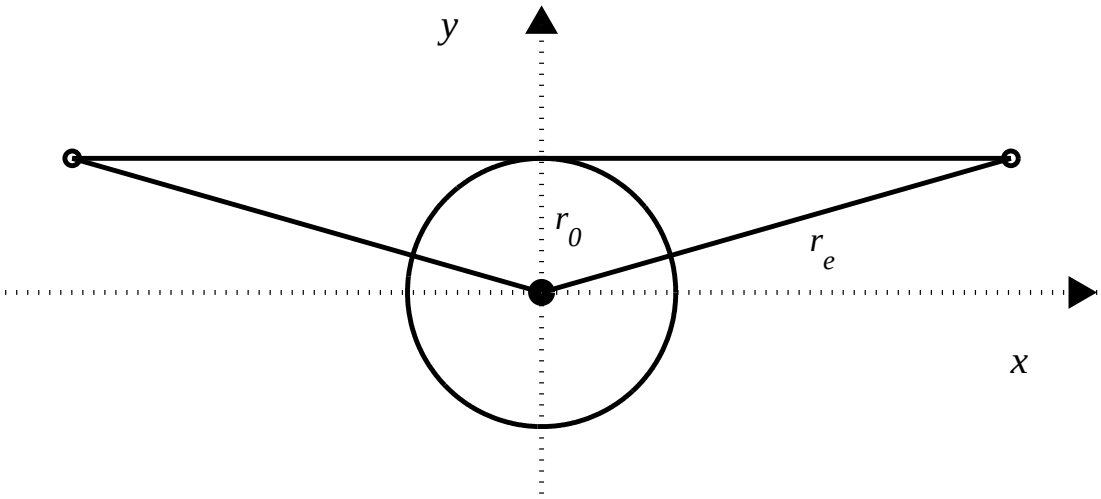

The delay can be calculated using the new refractive index, equation (2.11), and multiplying by ds so that

$$nds = \frac{r}{r-r_s}\sqrt{dr^2 + r(r-r_s)d\phi^2} = \frac{r}{r-r_s}\sqrt{1 + r(r-r_s)(\frac{d\phi}{dr})^2}dr.$$

Again, $(d\phi/dr)^2$ is given by the path equation (2.7). The time taken for the trip will be twice the time to go from the point of closest approach to the sun, r_0 to the earth's orbit, r_e, that is

$$T = \frac{2}{c}\int_{r_0}^{r_e} nds = \frac{2}{c}\int_{r_0}^{r_e} \frac{r}{r-r_s}\sqrt{1 + \frac{r(r-r_s)}{r^4(r_0-r_s)/r_0^3 - r(r-r_s)}}dr.$$

The integrand is infinite at $r = r_0$, so before integrating, we make the substitution $\cos(\psi) = r_0/r$. After rearrangement we get:

$$T = \frac{2r_0^2}{c}\int_0^{\arccos(r_0/r_e)} \frac{d\psi}{\cos^2\psi(r_0 - r_s\cos\psi)}\sqrt{\frac{(r_0 - r_s)(1+\cos\psi)}{(r_0 - r_s)(1+\cos\psi) - r_s\cos^2\psi}}. \tag{2.12}$$

This integrand is perfectly well behaved over the interval, so it can be integrated to arbitrary precision by using, for example, Gaussian Quadrature. As for the deflection, the delay is very small, so it is important to subtract the straight-line time before integrating. The straight-line time can be written as:

$$T_0 = \frac{2}{c}\sqrt{r_e^2 - r_0^2} = \frac{2r_0}{c}\int_0^{\arccos(r_0/r_e)} \frac{d\psi}{\cos^2\psi}. \tag{2.13}$$

The delay is obtained by subtracting equation(2.13) from equation(2.12) to give:

$$\triangle t = \frac{2r_0}{c}\int_0^{\arccos(r_0/r_e)} \frac{(1-\gamma)d\psi}{\gamma\cos^2\psi} \tag{2.14}$$

where

$$\gamma = \big(1 - (r_s/r_0)\cos\psi\big)\sqrt{1 - \frac{r_s\cos^2\psi}{(r_0 - r_s)(1+\cos\psi)}}$$

This expression (2.14) is now in a form that minimizes errors caused by subtraction of large terms. Performing this calculation in MatLab gives a delay of 129.0896086 μs. As for the deflection, this calculation can be performed to arbitrary precision, and accurately describes the delay predicted by general relativity.

For comparison, Weinberg (1972), pages 201 - 203, gives the following formula for the delay, to first order in r_s/r_0:

$$\triangle t = \frac{r_s}{c}\left[2\ln\left(\frac{r_e + \sqrt{r_e^2 - r_0^2}}{r_0}\right) + \sqrt{\frac{r_e - r_0}{r_e + r_0}}\right]. \tag{2.15}$$

This gives a delay of 129.0894053 μs. The fractional difference between this and the delay calculated above using equation (2.14) is:

$$\frac{129.0896086 - 129.0894053}{129.0896086} = 1.57\text{x}10^{-6},$$

which is of the same order as $r_s/r_0 = 2.95/696000 \simeq 4.24\text{x}10^{-6}$, as expected. Note that equation (2.15) is usually further approximated and simplified (Weinberg (1972), page 203, Kenyon (1990), pages 95-96) by saying that $r_0 << r_e$. This gives:

$$\triangle t = \frac{r_s}{c}\left[2\ln\left(\frac{2r_e}{r_0}\right) + 1\right],$$

which is significantly less accurate, giving a delay of 129.1350325 μs.

We now turn to a kinematic approach, and consider differential equations that relate position, velocity and acceleration. In a Newtonian system, the acceleration would be given by Newton's law of gravitational attraction, $\mathbf{g} = -c^2 r_s/2r^2\mathbf{e_r}$, with unit vector $\mathbf{e_r}$ pointing radially outward from the mass source. This simple formula is not appropriate for the present application, and a new form will now be derived from the present relativistic approach.

2.4 A New Acceleration Formula

By combining the metric equation (2.1) with the path equation (2.7) for a photon in a Schwarzschild orbit, the velocity and acceleration of the photon due to the nearby mass are now derived. Here the meaning is that of a coordinate acceleration. As a freely falling particle, the photon does not experience any locally measurable force. Beginning with the path equation (2.7), and making the substitutions

$$A = \frac{r_0 - r_s}{r_0^3} \text{ and } \mu(r) = 1 - \frac{r_s}{r}, \tag{2.16}$$

the path equation becomes

$$\left(\frac{dr}{rd\phi}\right)^2 = Ar^2 - \mu. \tag{2.17}$$

Next, considering equation (2.1), setting $dl^2 = 0$, $\theta = \pi/2$ and dividing through by dt^2, we have

$$c^2\mu^2 = \dot{r}^2 + \mu(r\dot{\phi})^2 \tag{2.18}$$

where $\dot{r} = v_r$ is the radial velocity component and $r\dot{\phi} = v_\phi$ is the tangential velocity component. Using the path equation (2.17), we can solve for v_r and v_ϕ in turn, to get:

$$v_r = \dot{r} = \pm c\mu\sqrt{1 - \frac{\mu}{Ar^2}} \tag{2.19}$$

$$v_\phi = r\dot{\phi} = \pm\frac{c\mu}{\sqrt{Ar^2}} \tag{2.20}$$

Thus the velocity vector of the photon along its path is

$$\boldsymbol{v} = v_r\boldsymbol{e_r} + v_\phi\boldsymbol{e_\phi} = \pm c\mu\left[\sqrt{1 - \frac{\mu}{Ar^2}}\boldsymbol{e_r} \pm \frac{1}{\sqrt{Ar^2}}\boldsymbol{e_\phi}\right].$$

To determine the acceleration vector, take the derivative with respect to time:

$$\boldsymbol{a} = \dot{v_r}\boldsymbol{e_r} + v_r\dot{\boldsymbol{e_r}} + \dot{v_\phi}\boldsymbol{e_\phi} + v_\phi\dot{\boldsymbol{e_\phi}}$$

In polar coordinates, the derivatives of the unit vectors are $\dot{\boldsymbol{e_r}} = \dot{\phi}\boldsymbol{e_\phi}$ and $\dot{\boldsymbol{e_\phi}} = -\dot{\phi}\boldsymbol{e_r}$, and so the acceleration components a_r and a_ϕ are

$$a_r = \dot{v_r} - \dot{\phi}v_\phi,$$

$$a_\phi = \dot{v_\phi} + \dot{\phi} v_r.$$

Differentiating v_r in equation (2.19) yields:

$$\dot{v_r} = \pm \frac{c\dot{r}}{r^2} \left[r_s \sqrt{1 - \frac{\mu}{Ar^2}} + \frac{\mu(2r - 3r_s)}{2Ar^2\sqrt{1 - \mu/Ar^2}} \right].$$

Equations (2.19) and (2.20) are now used to eliminate the square root terms, so that $\dot{v_r}$ simplifies to

$$\dot{v_r} = \pm \frac{1}{r^2} \left[\frac{r_s v_r^2}{\mu} + (r - \frac{3}{2} r_s) v_\phi^2 \right]$$

The radial acceleration component is therefore

$$a_r = \dot{v_r} - \dot{\phi} v_\phi = \dot{v_r} - \frac{v_\phi^2}{r} = \pm \frac{1}{r^2} \left[\frac{r_s v_r^2}{\mu} + (r - \frac{3}{2} r_s) v_\phi^2 \right] - \frac{v_\phi^2}{r}. \tag{2.21}$$

The acceleration must be related directly to the Schwarzschild radius r_s of the mass. There are two terms in equation (2.21) that do not have an r_s coefficient. These two terms cancel if the positive sign is chosen. Thus, the correct form for the radial acceleration is:

$$a_r = \frac{r_s}{r^2} \left[\frac{v_r^2}{\mu} - \frac{3v_\phi^2}{2} \right].$$

A similar treatment for tangential acceleration component yields

$$a_\phi = \dot{v_\phi} + \dot{\phi} v_r = \frac{r_s}{r^2} \frac{v_r v_\phi}{\mu}.$$

Thus the acceleration vector for a photon near a Schwarzschild mass is:

$$\boldsymbol{a} = \frac{r_s}{r^2} \left[[\frac{v_r^2}{\mu} - \frac{3v_\phi^2}{2}] \boldsymbol{e_r} + \frac{v_r v_\phi}{\mu} \boldsymbol{e_\phi} \right]. \tag{2.22}$$

It is interesting to note that the radius for light to remain in a circular orbit about

the mass can immediately be derived from this acceleration. In a circular orbit, there is no radial velocity, and so

$$\boldsymbol{a} = \frac{r_s}{r^2}\left[-\frac{3v^2}{2}\right]\boldsymbol{e_r} \tag{2.23}$$

In addition, an object moving in a circular orbit in a classical kinematical framework has centripetal acceleration vector

$$\boldsymbol{a} = -\frac{v^2}{r}\boldsymbol{e_r} \tag{2.24}$$

When equations (2.23) and (2.24) are equated, we obtain

$$r = \frac{3r_s}{2} \tag{2.25}$$

Thus, a photon at the '3/2' radius given in equation (2.25) is trapped in a circular orbit about the mass, in accordance with the known result predicted by general relativity (Carroll (2004), p 212).

2.4.1 Kinematic Ray Shooting

With known acceleration components, it is now possible to set up a standard system of differential equations for ray tracing in polar coordinates. The kinematical system is

$$\frac{d}{dt}\begin{bmatrix} r \\ \phi \\ v_r \\ v_\phi \end{bmatrix} = \begin{bmatrix} v_r \\ v_\phi/r \\ a_r + v_\phi^2/r \\ a_\phi - v_r v_\phi/r \end{bmatrix} \tag{2.26}$$

This new system (2.26) makes use of the new acceleration formula in equation (2.22). Such a system can be solved using forward integration. Initial conditions for the photon have initial position at perihelion of 696 000 kilometres about a mass with Schwarzschild radius of 2.95 kilometres, zero radial velocity, and tangential velocity $v_\phi = c/n = c\sqrt{\mu}$ to the right. The speed of light is taken to be $c = 300\,000$ kilometres/second. Using MatLab's ODE45 routine (an explicit Runge-Kutta 4-5 method) produces the path shown in Fig. 2.2 for the section shown; beyond this, the path is almost a straight line and so is not shown. The slope of the line between the last integration point before the photon reaches earth orbit, and the first point after is 1.74851634 ± 10^{-8} arcseconds. The time delay is calculated in the same integration, and is found to be 129.089609 ± 10^{-6} μseconds. The uncertainty is due to limitations on the precision of MatLab's ODE45 routine. Both of these values correspond well with the predictions from general relativity (as calculated above), more closely than the first order approximations, and use of a higher precision computation will allow a more accurate result, should such be required. Accuracy beyond first order is not commonly required, but these results give confidence that the acceleration vector presented here does accurately embody the effect on the photon due to a single Schwarzschild-type mass.

Using the values found for position and radial and tangential velocities when the photon reaches earth orbit, we can send the photon along the path from earth orbit past the sun and back out to earth orbit. The central section is shown in Fig. 2.3. Note that the scales differ by a factor of 10^6.

The values for the deflection angle and the Shapiro delay calculated by this forward integration ray shooting are compared with the predictions from general relativity and the usual first order approximations (as calculated earlier) in Table 2.1, and demonstrate that the kinematic ray shooting method presented in this chapter

FIGURE 2.2: Path of photon from perihelion, plotted in MATLAB using 2D kinematic ray shooting.

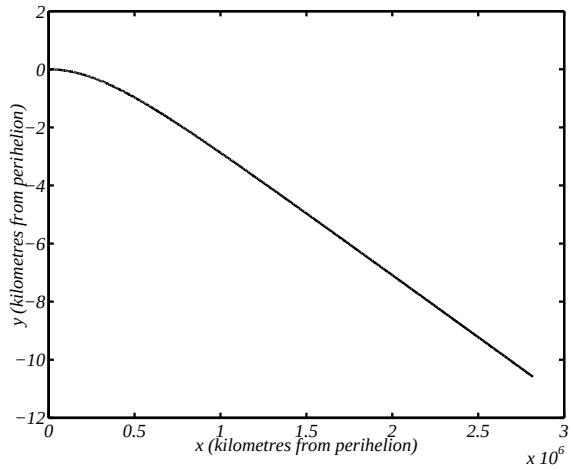

FIGURE 2.3: Path of photon past perihelion. The scales differ by a factor of 10^6.

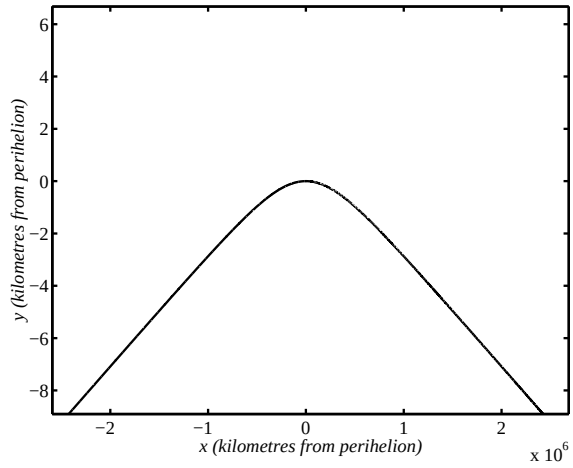

Approach	Deflection (arcsec)	Delay (μs)
Gen. Rel. prediction by integration along path (eqns. 2.9 and 2.14)	1.74851634161261	129.0896086
Usual approximations to first order in r_s/r_0 (eqns. 2.10 and 2.15)	1.74850913341648	129.0894053
Forward integration using new acceleration formula	1.74851634 ± 10^{-8}	129.089609 ± 10^{-6}

TABLE 2.1: A Comparison of the new method with accurate predictions from general relativity, and the common first order approximations.

is an accurate representation of the effect of the gravitational field of a single Schwarzschild body on the motion of a photon, giving us some confidence in using this method for more complicated systems.

2.4.2 Magnification Maps

When considering a multi-body system, such as a planetary system, it must be stressed that there is no known metric. That is, there is no known exact solution to Einstein's equations for such a system. Some sort of approximation is therefore required. Use of the 'weak-field metric' is one such approximation, as is the addition of the deflection angles due to each body (the method generally used in microlensing models). Here, we choose to approximate by adding the acceleration components due to each body in the system.

This approximation is analogous to the summation of acceleration components in a classical Newtonian regime. However, in the framework of General Relativity, there is no a priori justification for such an approach. In the case of the thin-lens approach, the contributions of deflection due to multiple masses are summed in a similar way, but this is a direct consequence of the linearised gravity approach, and so is justified (Bartelmann (2010), p.17). It is beyond the scope of this work to

provide justification for the current approximation, or to attempt to quantify the errors involved in doing so, but such a study would be an interesting and valuable topic for future research.

Having tested the radial and tangential acceleration components described above, it is a simple matter to set up a three dimensional ray tracing system for a planetary system. At each integration point along each ray, the acceleration components due to each massive body are calculated. This is done by a translation to put the massive body at the origin, followed by three rotations to place the photon's position vector and its velocity vector in the same plane as the massive body, with $\theta = \pi/2$. The radial and tangential velocities are then used to calculate the radial and tangential acceleration components. The three rotations are then reversed, and the resultant Cartesian acceleration components are added to the acceleration components due to any other masses in the system to determine the overall acceleration of the photon.

As a very simple (and artificial) example of this process, we first consider a two dimensional system, consisting of two very massive bodies in close proximity, and plot the path of the photon through this binary system. The smaller and larger stars represent bodies of 20 million and 50 million solar masses respectively (similar to the system described by Boroson and Lauer (2009), although in the present example we imagine that the system has decayed to the point where the black holes are only a billion kilometres apart). This example is purely to demonstrate the versatility of the present approach. We are making the gross simplification that the black holes are stationary throughout the period when the ray is passing through the system, and so the acceleration of the two masses towards each other is therefore being ignored. For the purpose of demonstrating the procedure used here, we are ignoring such limitations. The present model is clearly a coarse

FIGURE 2.4: Path of a photon through a super-massive binary black hole system. The black holes are indicated on the diagram with asterisks, and they are located at (-946.08,-315.36) and (0,23.652)

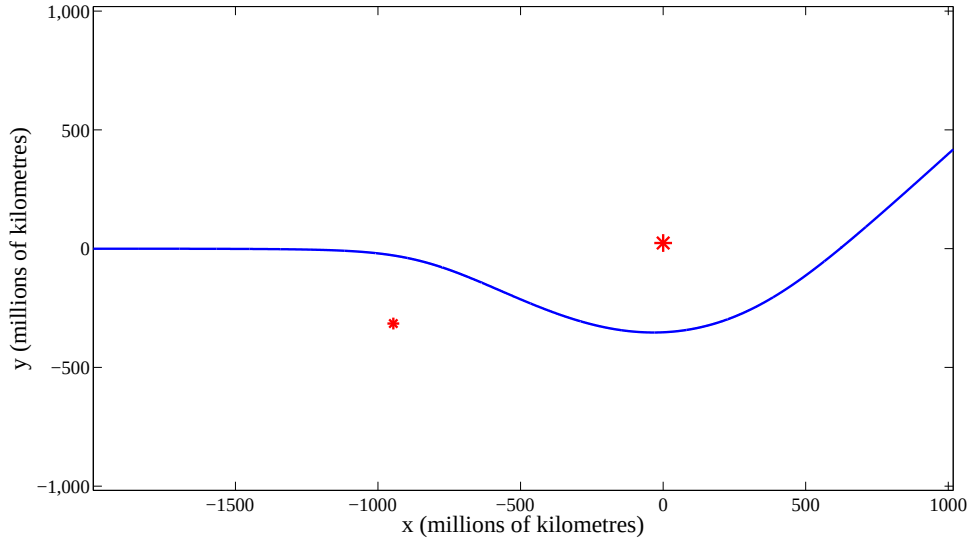

approximation in this extreme case. The light ray comes in from the far left, and is deflected by the summed acceleration components due to each mass. The path is shown in Fig. 2.4.

We now consider a more commonly modelled lensing system, the planetary lens. In describing a lensing system, it is common to use a parameter called the Einstein radius. This is the angular radius at which observers perfectly aligned with the point source and point lens would see a ring of light about the lens. Specifically, the system is designed as follows: a point source is at $(-8000, 0, 0)$ and the observer is at $(+8000, 0, 0)$. The lens star is placed at the origin, having Schwarzschild radius: $r_s = 99 * 10^{-8}$. A planet is placed at $(0, 0.1208, 0)$ (in micro-lensing terms, it is at 1.35 times the Einstein radius), with $r_s = 1 * 10^{-8}$. For simplicity in this model, we ignore the motion of the planet. Rays are sent through the system, near

the Einstein radius, and in the vicinity of the planet. Due to symmetry in the cases here, it is only necessary to calculate half the rays and plot the result both above and below the axis of symmetry. During the numerical integration, each ray is broken into several small sections, with the size of each section becoming smaller as the photon nears the lens star. This is important to ensure that the integration routine does not take too large a step and miss the strong deflection altogether. For the simulations presented in this chapter, each ray is broken into 36 segments. The result of this process is a light density map, or magnification map (that is points in (y, z) where the rays cross the plane $x = 8000$). These simulations were run on MatLab version 6.1, under Windows XP, on an Athlon 64 3500+ processor with 1GB of ram. Running times will be discussed as an indication, but no measures have been made to optimise the code for efficiency.

Fig. 2.5 shows the magnification map produced when a rectangular array of rays (222 by 205) is sent through the lens system. The bending of the light towards the planet is clearly visible. This, combined with the bending caused by the lens star, produces the characteristic diamond shape for a system with a single planet outside the Einstein radius (Wambsganss, 1997). The running time was 26 hours. In Fig. 2.6, many more rays have been used (approximately 106 000 rays). In order to view the resulting density, it is necessary to colour or shade regions according to how many rays pass through each small area. The code used to do this was 'smoothhist2d', (Perkins, 2006). The running time was approximately 50 hours. This result clearly shows the caustic diamond structure.

This diamond structure is the expected shape for the magnification map, and suggests that the method used here can be considered as an alternative method for modeling a thin lens.

FIGURE 2.5: Caustic structure due to planet with mass 1% of star's mass, located at 1.35 Einstein radii, using over 40,000 rays

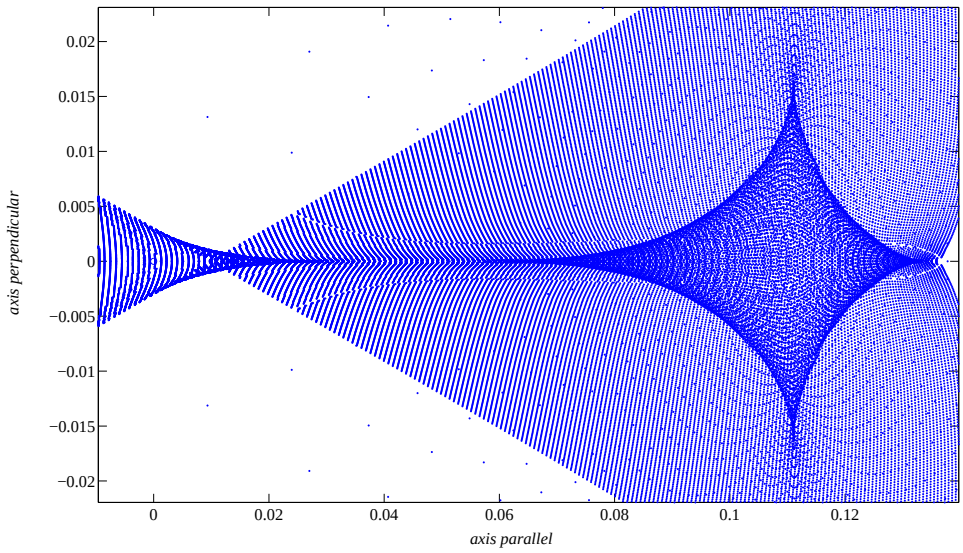

2.5 Conclusion and Discussion

We have considered the path of a photon near a Schwarzschild-type body. Using the Schwarzschild metric, a new refractive index has been derived. Integrating the angle along the path gives the total deflection angle, and integrating the new index along the path gives the travel time delay. These values for the delay time and deflection can be calculated, using the formulae here, to arbitrary precision. This is because these formulae are derived directly from the Schwarzschild metric. As a check, it was shown that the standard first order approximations used for the deflection and delay agree with these results to first order.

A new formula for acceleration of a photon was derived by combining the path equation with the Schwarzschild metric, and differentiating. This new acceleration formula was tested with a ray shooting approach, using the new refractive index to

FIGURE 2.6: Magnification density plot; same parameters as in Fig. 2.5, using 106000 rays

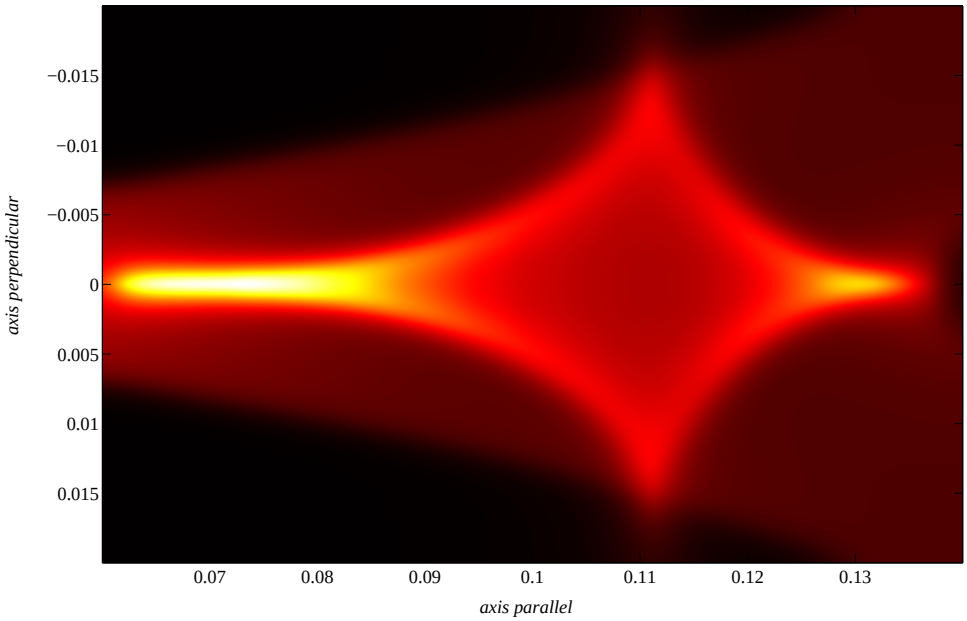

provide the initial conditions for the velocity components. The deflection and delay values were found to be in excellent agreement with the precise values calculated earlier.

By making the approximation that the acceleration on the photon is the sum of the individual acceleration components due to each massive body, a simple microlensing model was developed to demonstrate a use of the new acceleration formula for a binary system. Sample light fields on an observer plane have been computed using this new approach, and reproduce the expected figures. No attempt has been made here to speed computations, since that was not the purpose of the present work, but future developments may address such issues of computational efficiency. In the next chapter, an alternative approach will be pursued, an approximation

that leads to an analytic solution, allowing for much faster computation of light paths and magnification patterns.

In summary, this work provides a 'classical' way of accurately describing the gravitational effect on a photon due to a single mass, and provides an alternative method for approximating the course of a photon through a complicated mass distribution. The approach presented here provides an insight into the effect of gravitating bodies on light rays that can be grasped without requiring a deep understanding of general relativity, and yet is still quantitatively accurate for a single mass, and can be used for approximating more complicated systems. As for the standard thin lens 'deflection angle' method, this approach to gravitational lensing may be used by applied mathematicians, computer modellers and others without requiring specialist knowledge of general relativity. Because this approach retains the 'delay' information as well as the deflection, it might conceivably be useful in analysing systems where the time delay plays a role, such as a pulsar source being lensed, should we observe such an event. It is also hoped that the formulae presented here will prove useful in producing models of more complicated mass distributions, such as galaxy clusters. Such models could be produced using the same method used here, simply by adding more bodies to the model.

Chapter 3

Linear Approximation of Light paths near a non-rotating body

3.1 Introduction

In Chapter 2 new kinematic formulae were presented for ray tracing in gravitational lensing models. Such an approach can generate caustic maps, but is computationally expensive. Here, a linearized approximation to that formulation is presented. Although still complicated, the linearized equations admit a remarkable closed-form solution. As a result, linearized approximations to the caustic patterns may be generated extremely rapidly, and are found to be in good agreement with the results of full non-linear computation. The usual Einstein angle approximation is derived as a small angle approximation to the solution presented here.

For ease of reference, it is convenient to reproduce the acceleration vector, equation (2.22) derived in Chapter 2,

$$\boldsymbol{a} = \frac{r_s}{r^2}\left[\left[\frac{v_r^2}{\mu} - \frac{3v_\phi^2}{2}\right]\boldsymbol{e_r} + \frac{v_r v_\phi}{\mu}\boldsymbol{e_\phi}\right]. \tag{3.1}$$

and the kinematic system described there (2.26) is

$$\frac{d}{dt}\begin{bmatrix} r \\ \phi \\ v_r \\ v_\phi \end{bmatrix} = \begin{bmatrix} v_r \\ v_\phi/r \\ a_r + v_\phi^2/r \\ a_\phi - v_r v_\phi/r \end{bmatrix} \tag{3.2}$$

This system of equations can be solved numerically, although doing so is computationally expensive. In Chapter 2 this system was used to study the effect of a mass on a light ray, and showed that it could produce the caustic patterns expected from such a gravitational lens. The aim of the current chapter is to produce a linearized approximation to this, which will require much less computational processing.

3.2 Zeroth Order Solution

It is necessary first to derive the zeroth order solution $(R_0(t), \Phi_0(t))$ to the kinematic system (3.2). In this solution, the photon path is simply a straight line. This is obtained by setting $r_s = 0$, thus ignoring any acceleration due to the massive body. In this case, with the acceleration terms a_r and a_ϕ being zero,the kinematic equations for r and ϕ reduce to

$$\frac{\ddot{r}}{r} = \dot{\phi}^2 \text{ and } 2\dot{r}\dot{\phi} + r\ddot{\phi} = 0. \tag{3.3}$$

FIGURE 3.1: Photon path in empty space. $r(t)$ is the distance to the origin, r_0 is the distance from origin to perihelion.

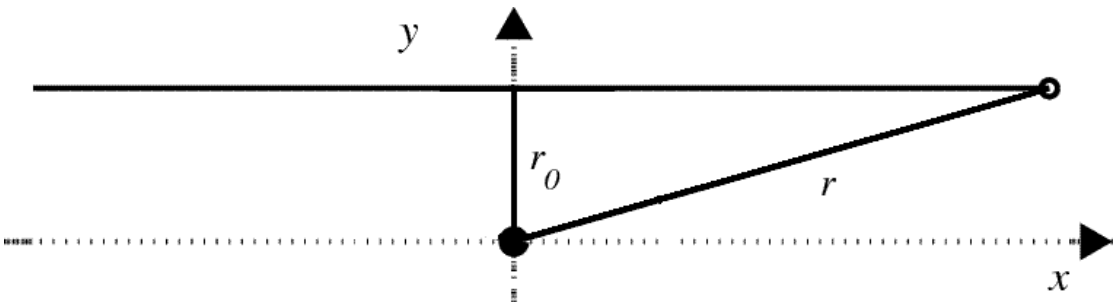

The second equation in (3.3) is readily rearranged to give $2\dot{r}/r = -\ddot{\phi}/\dot{\phi}$, and then integrated to show that $2\ln|r| = -\ln\left|\dot{\phi}\right| + \text{constant}$. Thus

$$\dot{\phi} = \pm c_1/r^2. \tag{3.4}$$

Substituting this into the left equation in (3.3) gives $\ddot{r} = c_1^2/r^3$. On multiplication by $2\dot{r}$ this yields $2\dot{r}\ddot{r} = 2c_1^2\dot{r}/r^3$, which can immediately be integrated to $\dot{r}^2 = -c_1^2/r^2 + c_2$. This is a first-order separable differential equation, and it has general solution

$$r(t) = \sqrt{c_2}\sqrt{(\frac{c_1}{c_2})^2 + (t - t_0)^2}$$

The minimum value of r is taken to be r_0 and to occur at $t = t_0$, so that $r_0 = c_1/\sqrt{c_2}$. Considering the straight path as in Fig. 3.1, we can identify $\sqrt{c_2} = c$, the speed of light in empty space. Thus the zeroth order solution for r becomes

$$R_0 = \sqrt{r_0^2 + (c(t - t_0))^2} \tag{3.5}$$

We can now calculate $\dot{\phi}$ from equation (3.4):

$$\dot{\phi} = \pm cr_0/r^2 = \pm \frac{cr_0}{r_0^2 + c^2(t-t_0)^2}. \tag{3.6}$$

Integration of equation (3.6) gives the zeroth order solution for ϕ

$$\Phi_0 = \pm \arctan\left(\frac{c(t-t_0)}{r_0}\right) + \text{constant}. \tag{3.7}$$

The sign will be negative for a ray passing the origin in a clockwise direction and positive for a ray passing in an anticlockwise direction. Note that R_0 is symmetric about $t - t_0$, while Φ_0 is antisymmetric. In what follows, it will be convenient to make the substitutions $u = (t-t_0)^2$, $D = r_0/c$ and $\tau = \sqrt{D^2 + u}$.

3.3 Linearisation

In this section, a linearized approximation to the equations describing the path of the photon is derived, based on the assumption that the path deviates only slightly from the straight line solution (R_0, Φ_0) obtained in Section 3.2. It is appropriate to define the small parameter $\epsilon = r_s/r_0$, where r_0 is the point of closest approach, and form the perturbation expansions

$$r = R_0 + \epsilon R_1 + O(\epsilon^2) \text{ and } \phi = \Phi_0 + \epsilon\Phi_1 + O(\epsilon^2). \tag{3.8}$$

Putting these into equation (3.1) gives two equations for the two components of the acceleration vector, the first of which is

$$\ddot{R}_0 + \epsilon\ddot{R}_1 - (R_0 + \epsilon R_1)(\dot{\Phi}_0 + \epsilon\dot{\Phi}_1)^2 = \epsilon\left[\frac{r_0\dot{R}_0^2}{R_0^2} - \frac{3r_0}{2}\dot{\Phi}_0^2\right] + O(\epsilon^2).$$

After expanding the left hand side in terms of τ and u, the zeroth-order terms cancel in view of equations (3.5) and (3.7). Retaining only terms to first order in ϵ gives

$$\tau^4 \ddot{R}_1 = D^2 R_1 + 2cD\tau^3 \dot{\Phi}_1 + r_0 u - \frac{3r_0}{2} D^2. \tag{3.9}$$

After rearranging for $\dot{\Phi}_1$, and differentiating and multiplying by τ^2, this becomes

$$2cD\tau^5 \ddot{\Phi}_1 = \tau^6 \dddot{R}_1 + \tau^4 \sqrt{u} \ddot{R}_1 - D^2 \tau^2 \dot{R}_1 + 3D^2 \sqrt{u} R_1 + r_0 \sqrt{u} (\tau^2 - \frac{15}{2} D^2). \tag{3.10}$$

The equation for the second component of the acceleration vector is

$$2\dot{r}\dot{\phi} + r\ddot{\phi} = \epsilon \frac{r_0 \dot{r} \dot{\phi}}{r}. \tag{3.11}$$

The perturbation series (3.8) are substituted into equation (3.11), and terms to order ϵ are retained. This gives rise to the linearized form

$$R_1 \ddot{\Phi}_0 + R_0 \ddot{\Phi}_1 = \frac{r_0 \dot{R}_0 \dot{\Phi}_0}{R_0} - 2\dot{R}_0 \dot{\Phi}_1 - 2\dot{R}_1 \dot{\Phi}_0 \tag{3.12}$$

Substituting the values for R_0 and Φ_0 from equations (3.5) and (3.7) gives

$$2cD\tau^5 \ddot{\Phi}_1 = 2D^2 r_0 \sqrt{u} + 4D^2 R_1 \sqrt{u} - 4BD\tau^3 \sqrt{u} \dot{\Phi}_1 - 4D^2 \tau^2 \dot{R}_1$$

Equating this with equation (3.10) allows the elimination of Φ_1 from the equation, arriving at a third-order differential equation for R_1:

$$\frac{\tau^6}{\sqrt{u}} \dddot{R}_1 + 3\tau^4 \ddot{R}_1 + \frac{3D^2 \tau^2}{\sqrt{u}} \dot{R}_1 - 3D^2 R_1 = r0(\tau^2 + \frac{9}{2} D^2) \tag{3.13}$$

To convert this into an equation in u, let $R(u) = R_1(t)$ and $R' = dR/du$. Then equation (3.13) becomes

$$8\tau^6 uR''' + 12\tau^4(\tau^2 + u)R'' + 6\tau^2(\tau^2 + D^2)R' - 3D^2R = r_0(\tau^2 + \frac{9}{2}D^2). \quad (3.14)$$

Equation (3.14) is the linearized differential equation for the deflection of the light ray from the zeroth-order solution. It is a third-order non-constant coefficient, inhomogeneous differential equation. Nevertheless it has a closed form solution, as will be found in the next section. Finally, by substituting this solution into equation (3.9), a solution for Φ_1 will be obtained. These solutions for R_1 and Φ_1, together with the zeroth-order solutions (3.5) and (3.7) will give the first-order approximation of the path of the photon in a system with a single massive body at the origin.

3.4 Closed Form Solution

Equation (3.14) has the form of an ordinary differential equation (ODE) with a regular singular point when $\tau^2 = D^2 + u \equiv 0$. This therefore suggests the change of variable $R(u) = \tau^n F(u)$. When this is substituted into equation (3.14), it is found appropriate to choose the index $n = -1$. Thus the change of variables $R(u) = F(u)/\tau$ reduces equation (3.14), after some algebra, to

$$8\tau^5 uF''' + 12\tau^5 F'' = r_0(\tau^2 + \frac{9}{2}D^2) \quad (3.15)$$

Remarkably, equation (3.15) is now a first order ODE in the variable F'', and admits of a closed form solution. This then promises the desired approximate method for calculating the intersection of the photon's path with the observer's

plane extremely rapidly, without the need for exact ray tracing as was used in Chapter 2. The equation can be re-written

$$u^{3/2}F''' + \frac{3}{2}u^{1/2}F'' = \frac{r_0\sqrt{u}}{8\tau^5}(\tau^2 + \frac{9}{2}D^2)$$

which can immediately be integrated once to

$$u^{3/2}F'' = \int \frac{r_0\sqrt{u}}{8\tau^5}(\tau^2 + \frac{9}{2}D^2)du$$

Using substitutions and integration by parts we can integrate twice more to find F to be

$$F = -r_0\sqrt{u}\ln(\sqrt{D^2+u} + \sqrt{u}) - \frac{r_0}{2}\sqrt{D^2+u} + 4k_1\sqrt{u} + k_2u + k_3$$

in which k_1, k_2, k_3 are constants of integration. Now $R(u) = F(u)/\tau$, so

$$R_1(t) = R(u) = -\frac{r_0}{2} + \frac{-r_0\sqrt{u}\ln(\sqrt{D^2+u} + \sqrt{u}) + 4k_1\sqrt{u} + k_2u + k_3}{\sqrt{D^2+u}}$$

It is a straight-forward matter to differentiate this expression three times with respect to t, and thus confirm that it does indeed satisfy equation (3.13).

This expression for R, in conjunction with equation (3.9) can be used to determine Φ_1, which is found to be

$$\Phi_1 \;=\; \frac{D}{c\tau^2}\left[r_0(\frac{\tau\sqrt{u}}{D^2} - \ln(\tau + \sqrt{u})) + 4k_1 + (k_2 - \frac{k_3}{D^2})\sqrt{u}\right] + \text{ constant.}$$

It can be shown that these formulae for R_1 and Φ_1 fulfil the first order kinematic

relations (3.9) and (3.12). The path equations may now be constructed to first-order in ϵ, using the equations in (3.8):

$$r = R_0 + \epsilon R_1 = c\tau - \frac{r_s}{2} + \frac{-r_s\sqrt{u}\ln(\tau+\sqrt{u}) + 4\epsilon k_1\sqrt{u} + \epsilon k_2 u + \epsilon k_3}{\tau} \tag{3.16}$$

The constants k_1, k_2 and k_3 can be identified in terms of r_s, r_0 and c, as follows. The path is symmetric about perihelion ($r = r_0$) so at that point, $t = t_0$ (and thus $u = 0$ and $\tau = r_0/c$), and so equation (3.16) becomes

$$r_0 = r_0 - \frac{r_s}{2} + \frac{\epsilon k_3}{r_0/c}$$

so

$$\epsilon k_3 = \frac{r_0 r_s}{2c}.$$

Also, at perihelion, r is a minimum so that $\dot{r} = 0$. Taking the derivative of equation (3.16) thus gives

$$4\epsilon k_1 = r_s \ln(D)$$

When u becomes very large, τ goes to $\sqrt{u}$, D/u goes to 0 and $\dot{r}$ goes to c, the constant speed of light far from the mass, so the derivative of equation (3.16) becomes:

$$\begin{aligned} c &= \frac{c\sqrt{u}}{\sqrt{u}} + \frac{1}{u^{3/2}}\left[\epsilon k_2\sqrt{u}(u) - \epsilon k_3\sqrt{u} - r_s\tau\sqrt{u} - r_s(r_0/c)^2\ln(\tau+\sqrt{u})\right] \\ &= c + \epsilon k_2 \end{aligned}$$

So $k_2 = 0$. Thus we can rewrite the equation for r as:

$$\begin{aligned} r &= c\tau - \frac{r_s}{2} + \frac{-r_s\sqrt{u}\ln(\tau+\sqrt{u}) + r_s\sqrt{u}\ln(r_0/c) + r_0 r_s/2c}{\tau} \\ &= \sqrt{r_0^2 + c^2 u} - r_s\left[\frac{1}{2} + \frac{\sqrt{u}\ln\left(\tau/D + \sqrt{u}/D\right) - r_0/2c}{\tau}\right] \end{aligned}$$

For readability, let $\psi(t)$ be the change in ϕ in the straight line solution for a ray passing the origin in an anti-clockwise direction, that is, $\tan\psi = -c\sqrt{u}/r_0$. Then

$$r = r_0\sec\psi - r_s\left[\frac{1-\cos\psi}{2} + \sin\psi\big[\ln\big(\frac{1+\sin\psi}{\cos\psi}\big)\big]\right] \tag{3.17}$$

Similarly for ϕ:

$$\phi = \phi_0 \pm \left\{\psi + \epsilon\left[\sin\psi - \frac{\sin 2\psi}{4} - \cos^2\psi\big[\ln\big(\frac{1+\sin\psi}{\cos\psi}\big)\big]\right]\right\}, \tag{3.18}$$

the positive or negative sign corresponding to the ray passing the mass in a clockwise or anti-clockwise direction, respectively. Now $\phi - \phi_0$ should be anti-symmetric about $t = t_0$ (that is, $\beta = 0$). Already, ψ is antisymmetric and has range $-\pi/2$ to $\pi/2$, and therefore so is $\sin\psi$ and $\sin 2\psi$. The symmetry of the logarithmic term may not be immediately obvious, but rearrangement yields

$$\ln\big(\frac{1+\sin\psi}{\cos\psi}\big) = \ln\big(\frac{\sqrt{1+\sin\psi}}{\sqrt{1-\sin\psi}}\big)$$

which is in fact antisymmetric, since its sign changes if ψ is replaced by $-\psi$. It can then also immediately be seen that r is symmetric about perihelion, as expected.

3.5 Application: Ray Shooting

We will first check that the first order formulae (3.17) and (3.18) for r and ϕ above give expected results for the well known deflection and delay for a photon passing close by the sun.

The usual approximation for the total deflection due to the sun (or any mass that is spherically symmetric, uncharged and having negligible angular momentum) is $2r_s/r_0$. The normal change in ϕ for an undeflected ray is π, so from equation (3.18), it can be easily seen that the deflection from perihelion ($\psi = 0$) out to infinity ($\psi = \pi/2$) is ϵ, so the total deflection for a photon passing close to the sun is $2\epsilon = 2r_s/r_0$, in agreement with the standard approximation.

The first order approximation for the Shapiro delay is more involved. As in Chapter 2 (where the precise delay was found to be 64.5448043 μs, for each leg of the journey from perihelion to earth orbit), we consider a photon having perihelion at 696 000 km, and reaching earth orbit at $1.5 * 10^8$ km. The sun's Schwarzschild radius is taken to be 2.95 km. We find that a time of 499.99468211573345 seconds in equation (3.17) gives a value for r of the required $1.500000000 * 10^8$ km. The 'straight line' time for light to travel from perihelion to the earth, without any gravitational effect, is $\sqrt{r_e^2 - r_0^2}/c = 499.9946175710294$ seconds, giving a delay of 64.54470398μseconds. Weinberg (1972), (p.202) uses the standard Schwarzschild coordinates so the result in this chapter can be compared directly with his approximation:

$$\triangle r \;=\; r_s \ln\left[\frac{r + \sqrt{r^2 - r_0^2}}{r_0}\right] + \frac{r_s}{2}\sqrt{\frac{r - r_0}{r + r_0}} \tag{3.19}$$

To calculate the delay, Weinberg then divides this distance by c, which, with the values used here for r, r_0, and r_s, gives a delay of 64.54470267 μs. In fact, as shown in Chapter 2, the apparent speed of light in this Schwarzschild coordinate system (which corresponds to a standard spherical system plus time as measured by an observer at rest far from the origin) is actually $c(1 - r_s/r)\sqrt{1 + r_s r_0^3/r^3(r_0 - r_s)}$. While the measured speed of light for any local observer will always be c, the time delay represents the increased travel distance (in a curved Space–time model) or the retardation of light (in a flat space model, such as the standard spherical coordinate system). Interestingly, dividing $\triangle r$ in equation (3.19) by this value for the speed of light brings this delay to 64.54470394 μs, which is much closer to the delay from the first order approach presented in this chapter. In any case, to first order, the first order approximation in this chapter agrees with Weinberg's first order approximation.

Next the new formulae are used to produce the caustic magnification patterns typical of a planetary system. Considering a photon with known position and velocity components in plane polar coordinates, the solution in equations (3.17) and (3.18) may be differentiated to give

$$\frac{\dot{r}}{c} = \sin\psi - \frac{r_s \cos\psi}{2r_0}\left[\frac{\sin 2\psi}{2} + \sin\psi + \cos^2\psi \ln\left[\frac{1+\sin\psi}{\cos\psi}\right]\right] \quad (3.20)$$

$$\frac{\dot{\phi}}{c} = \mp\frac{\cos^2\psi}{r_0}\left[1 - \frac{r_s}{r_0}\left(\frac{\cos 2\psi}{2} - \sin(2\psi)\ln\left[\frac{1+\sin\psi}{\cos\psi}\right]\right)\right] \quad (3.21)$$

For a photon at a distance L from the mass, without loss of generality, the coordinate system can be rotated so that the source is at $(-L,0)$ and the positive angle α indicates the angle from the x-axis to the tangent vector of the ray, as in Fig. 3.2. Then the ray is passing the mass in a clockwise direction, which indicates the

positive sign in equation (3.18) and the negative sign in equation (3.21). In that case, the point $(-L,0)$ must lie on the curve at some time ψ_0. So equations (3.17) and (3.18) reduce to

$$L = r_0 \sec\psi_0 - r_s\left[\frac{1-\cos\psi_0}{2} + \sin\psi_0 \ln\big[\frac{1+\sin\psi_0}{\cos\psi_0}\big]\right] \tag{3.22}$$

$$\pi = \phi_0 + \left\{\psi_0 + \epsilon\left[\sin\psi_0 - \frac{\sin 2\psi_0}{4} - \cos^2\psi \ln\big[\frac{1+\sin\psi_0}{\cos\psi_0}\big]\right]\right\} \tag{3.23}$$

at that point. The third equation specifies the initial angle α of the ray: $|\dot{r}\tan\alpha| = r|\dot{\phi}| = L|\dot{\phi}|$. This is combined with equations (3.20) and (3.21) to give

$$\begin{aligned}\tan\alpha&\left\{\sin\psi_0 - \frac{r_s\cos\psi_0}{2r_0}\left[\frac{\sin 2\psi_0}{2} + \sin\psi_0 + \cos^2\psi_0 \ln\big[\frac{1+\sin\psi_0}{\cos\psi_0}\big]\right]\right\}\\ &= \mathrm{sign}(\phi_0)L\frac{\cos^2\psi_0}{r_0}\left[1 - \frac{r_s}{r_0}\left(\frac{\cos 2\psi_0}{2} - \sin 2\psi_0 \ln\big[\frac{1+\sin\psi_0}{\cos\psi_0}\big]\right)\right]\end{aligned} \tag{3.24}$$

The three parameters r_0, ϕ_0 and ψ_0 are thus determined as the solutions to the three algebraic equations (3.22)-(3.24). Consistently with the perturbation expansions (3.8), a solution is now obtained to equations (3.22)-(3.24), accurate to first order in r_s. At zeroth order, the approximation would simply be

$$r_0 = L\sin\alpha; \quad \phi_0 = \alpha + \pi/2; \quad \psi_0 = -\alpha + \pi/2$$

and is obtained by setting $r_s = 0$. The first order solutions to (3.22)-(3.24) are now determined in the form

$$\begin{aligned} r_0 &= L\sin\alpha + r_s R_1 + O(r_s^2) \\ \phi_0 &= \alpha + \pi/2 + r_s\Phi_1 + O(r_s^2) \\ \psi_0 &= -\alpha + \pi/2 + r_s\Psi_1 + O(r_s^2) \end{aligned} \tag{3.25}$$

Equations (3.25) are substituted into equations (3.22)-(3.24) and solved for the three unknowns R_1, Φ_1 and Ψ_1 to give

$$r_0 = L\sin\alpha + r_s\frac{\sin^3\alpha - 1}{2} + O(r_s^2)$$

and

$$\phi_0 = \pi/2 + \alpha - r_s\frac{2+\sin^2\alpha}{2L\sin\alpha} + O(r_s^2)$$

At some later time, say $\psi = \psi_2$, the ray crosses the observer's plane. For the purposes of simplifying the mathematics, suppose that the observer's plane is the same distance from the mass as the source, but on the other side, that is, at $x = L$. Considering Fig. 3.3, the following first order approximations will be used:

$$\begin{aligned} r_2 &= L\sqrt{1+4\tan^2\alpha} + r_s R_2 + O(r_s^2) \\ \phi_2 &= \arctan(2\tan\alpha) + r_s\Phi_2 + O(r_s^2) \\ \psi_2 &= \arctan(2\tan\alpha) - \alpha - \pi/2 + r_s\Psi_2 + O(r_s^2) \end{aligned}$$

These approximations for r and ϕ are implemented in equations (3.17) and (3.18).

FIGURE 3.2: Photon path from source at $(-L, 0)$. The point of closest approach (r_0, Φ_0) is determined to first order.

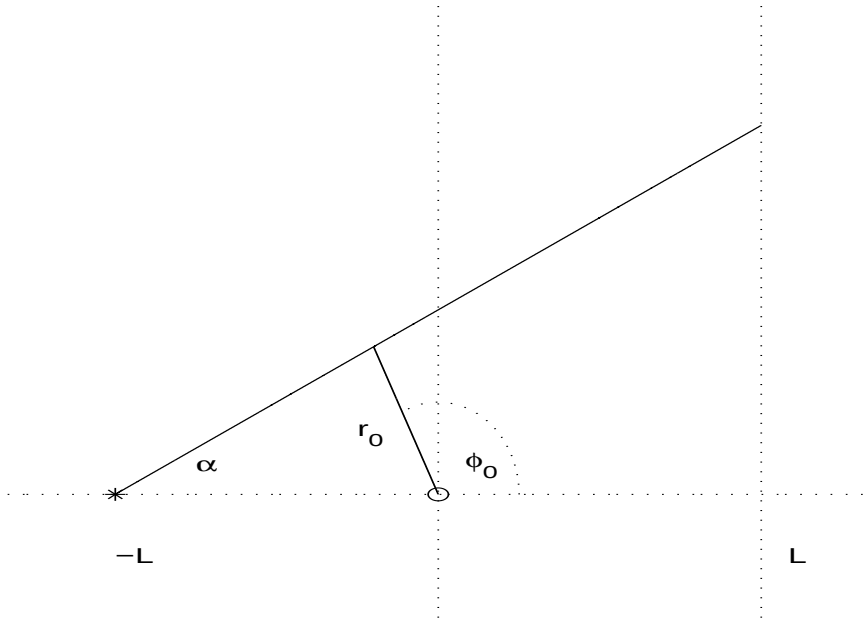

A third equation is given by the path crossing the observer's plane at $x = L$, that is, $L = r_2 \cos\phi_2$. Again, having three equations and three unknowns, the system is solved for R_2, Φ_2 and Ψ_2 to first order in r_s. The results for R_2 and Φ_2 are:

$$R_2 = -\frac{\cos\alpha(2+3\sin^2\alpha)\sqrt{1+3\sin^2\alpha}+2+5\sin^2\alpha+\sin^4\alpha}{\cos^2\alpha(1+3\sin^2\alpha)}$$

and

$$\Phi_2 = -\frac{\cos\alpha(2+3\sin^2\alpha)\sqrt{1+3\sin^2\alpha}+2+5\sin^2\alpha+\sin^4\alpha}{2L\sin\alpha(1+3\sin^2\alpha)^{3/2}}$$

FIGURE 3.3: Photon path from source at $(-L, 0)$ to observer's plane at $x = L$. The point of intersection with the observer's plane (r_2, Φ_2) is determined by the linearised equations.

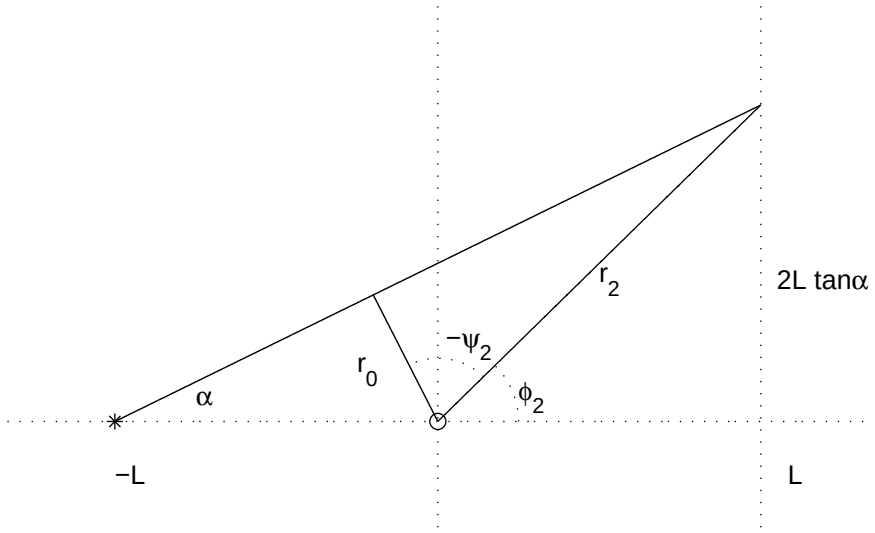

This expression enables easy calculation of the position at which the photon crosses the observer's plane, being at $(L, r_2 \sin \phi_2)$.

As this is a first order solution, we will now compare the results with those of the usual first order approximation, where the photon's path is taken to be two straight lines with a deflection angle of $2r_s/r_0$. Calling the deflected distance in the y component at the observer's plane, $\triangle y$, and considering Fig. 3.4, the values for $\triangle y$ predicted by the usual formula will be compared with the one presented in this chapter.

Calculating the deflection $\triangle y$ using the standard deflection formula $2r_s/r_0$ gives the result $\triangle y = 2r_s(1+\sin^2\alpha)/\cos^2\alpha \sin\alpha + O(r_s^2)$. This is represented in Fig. 3.5, which shows $\triangle y/r_s$ against values of α, as a dotted curve. The deflection predicted

in this chapter is $\triangle y = r_2 r_s \Phi_2 = r_s L \Phi_2 (1 + 3\sin^2\alpha)/\cos^2(\alpha) + O(r_s^2)$, which is shown in Fig. 3.5 as a solid curve. The two values agree for small values of α, but diverge for larger values. The reason for this becomes apparent by considering that when $\alpha = \pi/2$, the photon is 'starting' at perihelion, so it has already been deflected by half the total expected value, so the remaining deflection should only be r_s/r_0, according to the standard deflection method. This half deflection value is plotted as a dashed curve. It can be seen that the formula presented in this chapter accounts well with both formulae, as it agrees closely with the standard formula for small α (top panel in Fig. 3.5)and with half that amount for large α (bottom panel in Fig. 3.5).

As the stated aim of this exercise was to provide a faster method for generating caustic images than the previous kinematic method, it is important to compare the processing time using the new method, the previous kinematic method, and the simple angle change method. Fig. 3.6 was produced using the three different methods. Fig. 3.6(a) shows the caustic produced using the standard thin lens formula, Fig 3.6(b) used the linearised approach presented in the current chapter, and Fig. 3.6(c) was produced using the forward integration method of Chapter 2. Processing time using the kinematic ray tracing method was approximately 3000 seconds. Using the method in this chapter and the simple angle change method took 0.485 seconds and 0.468 seconds, respectively, on the same computer system. So the method in this chapter is some 6000 times faster than the ray tracing method, but still slightly slower than the simple angle method.

The planetary configuration is the same as used in Chapter 2: a point source is at $(-8000, 0, 0)$ and the observer is at $(+8000, 0, 0)$. The lens star is placed at the origin, having Schwarzschild radius: $r_s = 99 \times 10^{-8}$. A planet is placed at $(0, 0.1208, 0)$ (1.35 times the Einstein radius), with $r_s = 1 \times 10^{-8}$. For simplicity,

FIGURE 3.4: Two approaches for determining the deflection at the observer's plane, $x = L$. The total deflection $\triangle y$ can be determined by simple geometry either by the deflection from straight line by angle $2r_s/r_0$ (Einstein angle), or by the method presented in this chapter where the photon is deflected from the straight line solution by $r_s\Phi_2$, relative to the origin.

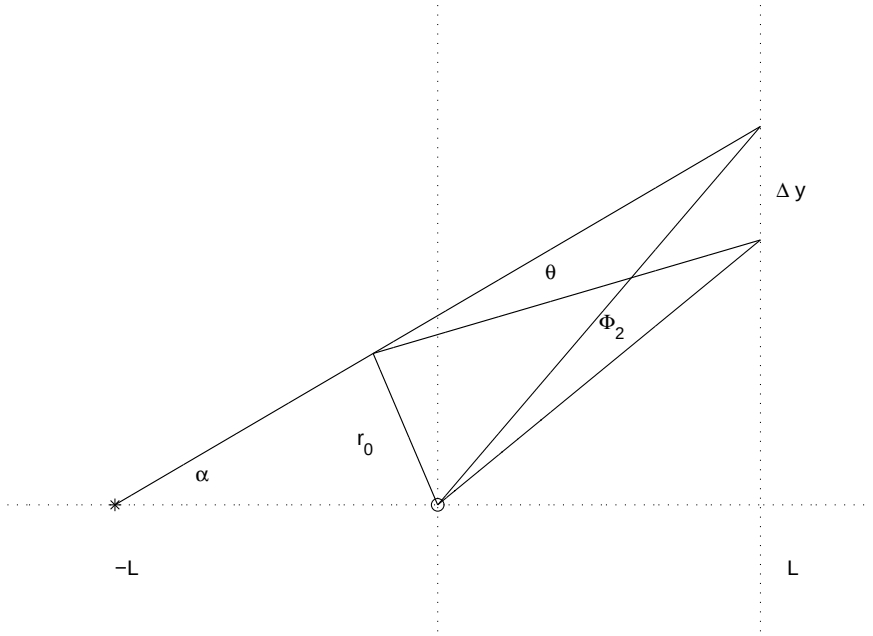

the motion of the planet is ignored. Rays are sent through the system, near the Einstein radius, in the vicinity of the planet. Due to symmetry in the cases here, it is only necessary to calculate half the rays and plot the result both above and below the axis of symmetry.

Using one of these magnification maps, it is a straight-forward procedure to generate a light curve (magnification over time), corresponding to a chosen path across the map. This is done by sampling the number of light rays passing through a narrow strip of the magnification map. For a simple point-source-point-lens system

FIGURE 3.5: Comparison of deflection predicted by the two different first-order approximations. The approach presented here is represented by a solid curve. The dotted curve represents the Einstein angle deflection formula, which agrees closely for small α (top panel). The dashed curve represents the half Einstein deflection formula, suitable for a photon 'starting' at perihelion. This curve agrees closely for large values of α (bottom panel). α is the initial angle of the light ray. $\alpha = 0$ would represent a light ray directed straight towards the lensing mass, $\alpha = \pi/2$ would represent a light ray initially tangential to the lensing mass. For typical lensing observations, α is very small.

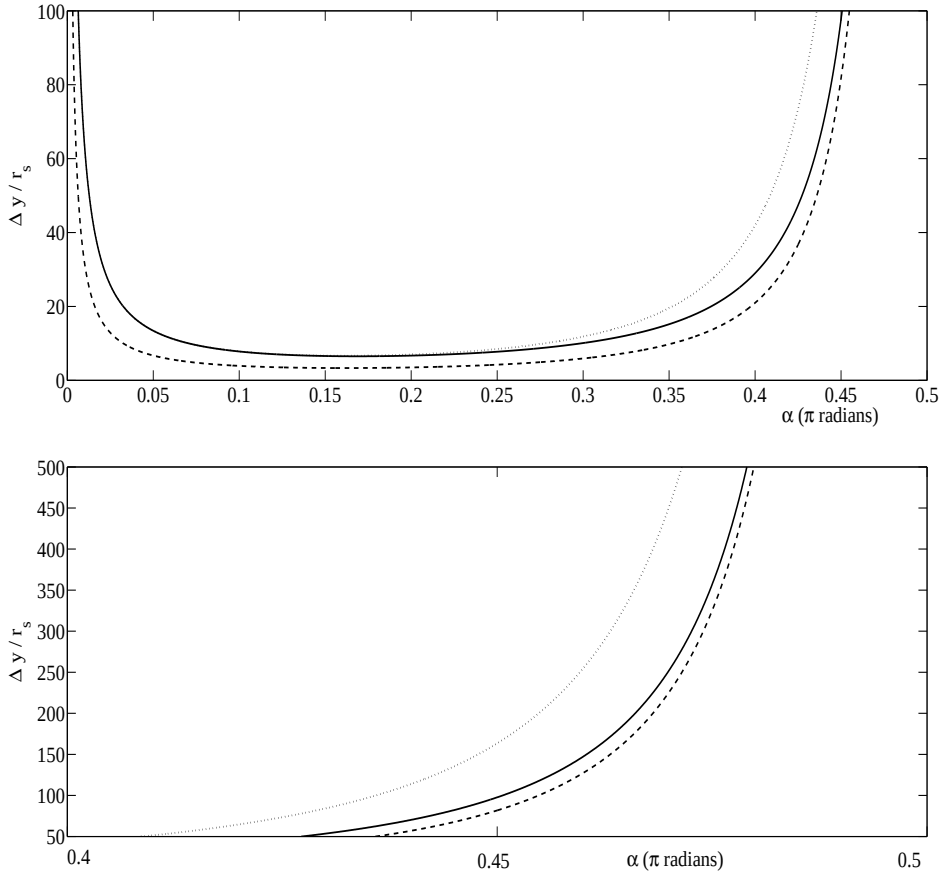

FIGURE 3.6: The caustic pattern for a single planetary system, the planet being at 1.35 Einstein radii. The three figures show calculations based on: (a) the standard thin lens formula; (b) the linearised method of this chapter; (c) forward integration using the full acceleration formula of Chapter 2.

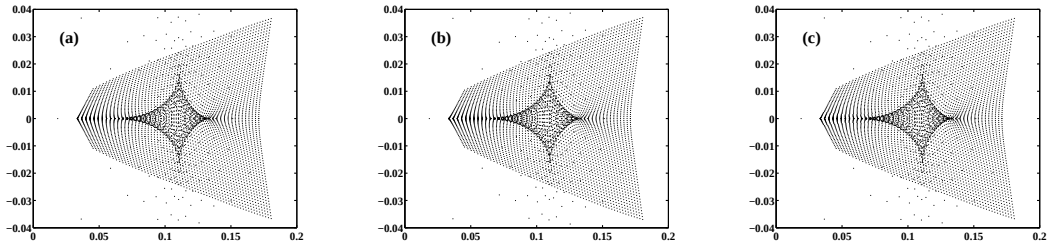

(PSPL), the light curve has a smooth symmetric form, whereas a binary lensing system may produce significant deviations from the simple light curve, although these are typically of short duration, depending on the relative speed of source, lens and observer. A comparison of such light curves is shown in Fig. 3.7. The upper panel shows a light curve due to the simple PSPL magnification map, and the lower panel shows the deviation due to the caustic structure in Fig. 3.6.

3.6 Conclusion and Discussion

In this chapter, we have considered a linearization of the kinematical system of equations discussed in Chapter 2. This gives a difficult, although linear, differential equation of third order, with non-constant coefficients. Remarkably, this equation admits an exact solution in closed form. This has been presented here, and the corresponding path equations have been described. This resulted in the sought-after decrease in processing time for producing magnification maps due to planetary systems, and has been found to be in good agreement with the results of ray tracing in the fully non-linear model of Chapter 2. Although this approach

FIGURE 3.7: Typical light curves for point-source-point-lens model (left), and for a binary system (right). The horizontal axis "Time" corresponds to the distance that the observer has travelled across the magnification map. Intensity is relative to the un-lensed intensity of the background star.

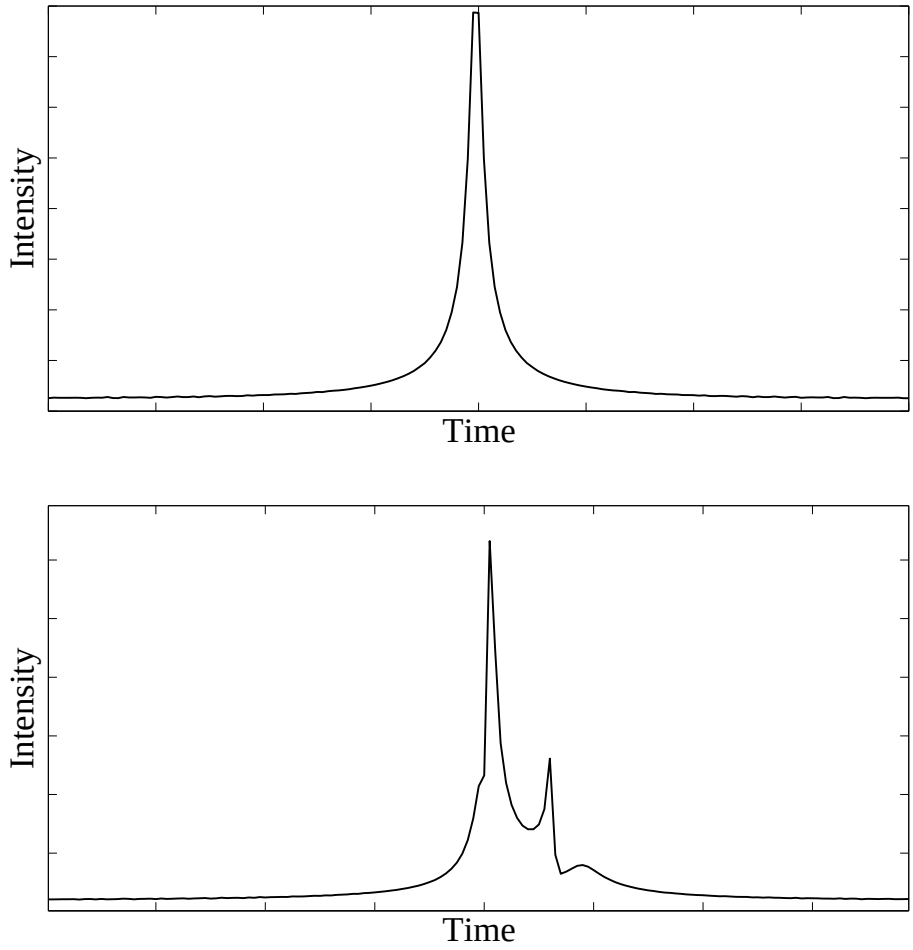

in some sense repeats the rapid approximate results already available with other methods, such as the thin lens formula of Wambsganss (1997), it nevertheless does so in an elegant and coherent fashion from the full kinematic equations, without the need to assume that deflections are confined only to a single plane containing the mass. The thin lens formula appears as a small angle approximation to the solution presented here. That being so, the method presented here can never be quite as fast as the thin lens method, due to the fact that the terms in the thin lens method formula are a subset of the terms in the formula derived here.

For small angles (which covers pretty much all observable lensing events), the thin lens method can be seen to be an excellent approximation to the approach presented here. Nevertheless, the approach of this chapter represents a rigorous and formal linearization of the non-linear ray path equations arising from the use of the Schwarzschild metric. As such, this approach can be viewed as a novel formal foundation for the usual thin lens formula. Since the resulting approximation here gives rise to a linear differential equation, the superposition principle allows systems containing multiple masses to be treated by simple addition of their effects.

Chapter 4

Rotating lenses

4.1 Introduction

In Chapter 1, lensing models were discussed and it was noted that the simplest model uses a thin-lens approach, deflecting the photon's path by the deflection angle predicted by Einstein (1936). In Chapter 2 a new approach was taken, in which the Schwarzschild metric was used to derive kinematic type laws for the propagation of light rays through a lensing system. It was found that the acceleration vectors thus derived gave results in close agreement with those obtained using the simpler model described above. In Chapter 3 a linearized approximation was considered, in which the light rays were assumed to deflect only slightly from an otherwise straight-line path. These linearized equations were shown to admit an exact closed-form solution which agreed well with the fully non-linear simulations.

In this chapter, the approach of Chapter 2 is generalized to include the effects of relativistic frame dragging due to rotation of the lensing object, as described by

the Kerr metric. The Kerr geodesic equations for massless particles are used to derive an acceleration vector in both Boyer-Lindquist and Cartesian coordinates. A kinematic description is given where it is found that converting to Cartesian co-ordinates simplifies the description of the light paths, by removing all acceleration terms at zeroth order. As a special case, the Schwarzschild acceleration due to a non-rotating mass has a particularly simple and elegant form in Cartesian coordinates. The non-rotating (Schwarzschild) case is examined in the new coordinate system, and rotation effects, which become significant at second order in the Schwarzschild radius, are considered. Using forward integration, these equations are used to plot the caustic pattern due to a system consisting of a rotating point mass with a smaller non-rotating planet. Additionally, first and second order approximations to the paths are identified, which allow for fast approximations of paths, deflection angles and travel-time delays. Finally, application to delay of pulses in a binary pulsar model is presented, followed by concluding remarks and an appendix containing equations relevant to this chapter.

4.2 Light Rays in a Kerr System

The Kerr metric describes spacetime outside an uncharged point mass, rotating or otherwise. The Schwarzschild solution is contained as a special case wherein the mass has no angular momentum. Such a solution has spherical symmetry, whereas for a rotating body, the system is axi-symmetric only. For any light path other than one confined to the equatorial plane, a fully three dimensional description of the path is required. This is different than for the Schwarzschild case, where any path is confined to a plane, and can thus be treated as a two dimensional problem. We therefore begin with the Kerr metric given in Boyer-Lindquist coordinates

(the conversion is described in Section 4.2.1 below), as written in Chandrasekhar's thorough mathematical treatment of black holes (Chandrasekhar, 1983).

$$\begin{aligned} dl^2 &= \frac{\Delta}{\rho^2}[dt - (a\sin^2\theta)d\phi]^2 - \frac{\sin^2\theta}{\rho^2}[(r^2+a^2)d\phi - adt]^2 \\ &- \frac{\rho^2}{\Delta}(dr)^2 - \rho^2(d\theta)^2. \end{aligned} \tag{4.1}$$

From this metric, the equations of motion can be derived. In this thesis, we are interested in the paths of light rays, so we consider the null geodesics $dl = 0$ for a Kerr spacetime (Chandrasekhar (1983), pp. 346-7):

$$\rho^4\dot{r}^2 = r^4 + (a^2 - L^2 - Q)r^2 + r_s r(Q + (L-a)^2) - a^2Q \tag{4.2}$$

$$\rho^4\dot{\theta}^2 = Q + a^2\cos^2\theta - L^2\cot^2\theta \tag{4.3}$$

$$\rho^2\dot{\phi} = \frac{1}{\Delta}(r_s a r + \frac{(\rho^2 - r_s r)L}{\sin^2\theta}) \tag{4.4}$$

$$\rho^2\dot{t} = \frac{1}{\Delta}((r^2+a^2)^2 - r_s a r L). \tag{4.5}$$

Here, the Schwarzschild radius is $r_s = 2MG/c^2$, t is the time coordinate in the reference frame of the mass, $a = J/Mc$ is the angular momentum term, and the dot indicates differentiation by a parameter, which we will call τ'. The other symbols are defined as: $\rho^2 = r^2 + a^2\cos^2\theta$; $\Delta = r^2 + a^2 - r_s r$; M is the mass of the body; and J is the angular momentum of the body. We are using geometrized units, that is, $c = G = 1$. Finally, L and Q are constants of the motion, related closely to the angular momentum of the particle. The first of these, L, comes from the first integral of the Euler-Lagrange equation for $\dot{\phi}$, and the second, Q, is Carter's

constant, which is derived from the separation of the Hamilton-Jacobi equation for geodesic motion (Chandrasekhar (1983), p. 342).

4.2.1 Acceleration Components

Solving equations (4.2) and (4.3) for $\dot{r}$ and $\dot{\theta}$ introduces square roots, for which the sign ($\pm$) is ambiguous (that is, either sign may be chosen). Additionally, it was found that numerical integrators such as the Runge-Kutta method find singular solutions such as closed orbits when integrating these equations, and so do not always find the path of unbound photons. To remove these difficulties, we will take derivatives, producing acceleration components which have a simpler form than the first derivatives. As the parameterisation is arbitrary, for simplicity we first re-parameterise in order to remove the ρ^2 terms at the beginning of each equation. We choose a parameter τ such that $r^2\frac{d}{d\tau} = \rho^2\frac{d}{d\tau'}$. This has the result that each instance of ρ on the left of the geodesic equations above becomes r. Re-using the dot-notation for $d/d\tau$ and differentiating gives the following equations:

$$\ddot{r} = \frac{L^2+Q-a^2}{r^3} - \frac{3r_s}{2r^4}(Q+(L-a)^2) + \frac{2a^2Q}{r^5} \tag{4.6}$$

$$\ddot{\theta} = \frac{\cos\theta}{\sin^3\theta}(L^2 - a^2\sin^4\theta) - \frac{2\dot{r}\dot{\theta}}{r} \tag{4.7}$$

$$\ddot{\phi} = \frac{a\dot{r}}{r^2\Delta^2}(r_s a^2 - r_s r^2 + aL(2r - r_s)) - \frac{2L\cos\theta}{r^2\sin^3\theta}\dot{\theta} - \frac{2\dot{r}\dot{\phi}}{r} \tag{4.8}$$

In order to describe the path of a particle through a system consisting of more than a single body at the origin, it is convenient to express the acceleration components in Cartesian co-ordinates. The conversion is given by the following substitutions

(Chandrasekhar (1983), pp. 306-7):

$$\begin{aligned} x &= (r\cos\widetilde{\varphi} + a\sin\widetilde{\varphi})\sin\theta \\ y &= (r\sin\widetilde{\varphi} - a\cos\widetilde{\varphi})\sin\theta \\ z &= r\cos\theta \end{aligned} \tag{4.9}$$

where $\dot{\widetilde{\varphi}} = \dot{\phi} - a\dot{r}/\Delta$. These equations provide an implicit definition of r as:

$$r^4 - r^2(x^2 + y^2 + z^2 - a^2) - a^2z^2 = 0$$

Notice that if there is no rotation, that is, $a = 0$, then this degenerates to a conversion from spherical co-ordinates, as expected. Differentiating the first equation in (4.9) twice gives the following expression for $\ddot{x}$:

$$\begin{aligned} \ddot{x} &= \frac{1}{a^2+r^2}\left[(x + \frac{r_s a y}{\Delta})(r\ddot{r} + \frac{a^2 - r^2}{a^2 + r^2}\dot{r}^2) + r\dot{r}\big(\dot{x} + \frac{r_s a\dot{y}}{\Delta} - \frac{r_s a(2r - r_s)y\dot{r}}{\Delta^2}\big)\right] \\ &- \dot{y}\dot{\phi} - y\ddot{\phi} - \frac{x\dot{\theta}^2}{\sin^2\theta} + \frac{\dot{x}\dot{\theta} + x\ddot{\theta}}{\tan\theta}. \end{aligned} \tag{4.10}$$

In this equation, $\dot{r}$, $\dot{\theta}$ and $\dot{\phi}$ are obtained from the conversion equations (4.9) by differentiation. A similar approach for y and z will give expressions for $\ddot{y}$ and $\ddot{z}$ respectively. Substituting in equations (4.6)-(4.8) for $\ddot{r}$, $\ddot{\theta}$ and $\ddot{\phi}$ and simplifying

leads to a system of the form

$$\begin{aligned}
\ddot{x} &= \frac{-3r_s x(L^2+Q)}{2r^5} + aF_x(x,y,z,\dot{x},\dot{y},\dot{z}) \\
\ddot{y} &= \frac{-3r_s y(L^2+Q)}{2r^5} + aF_y(x,y,z,\dot{x},\dot{y},\dot{z}) \\
\ddot{z} &= \frac{-3r_s z(L^2+Q)}{2r^5} + aF_z(x,y,z,\dot{x},\dot{y},\dot{z})
\end{aligned} \tag{4.11}$$

The constant a has a valid range from $-r_s/2$ to $r_s/2$. It is therefore reasonable to say that the angular momentum term a is of the same order of magnitude as the Schwarzschild radius r_s. It may then be said that because the functions F_x, F_y and F_z are of order r_s, the first term in each of the equations in (4.11) is of first order, and the remainder is second order and higher. The full acceleration components in equation (4.11) are given in Section 4.7.

4.3 Schwarzschild Acceleration in the Cartesian Co-ordinate System

We can see that for the non-rotating (Schwarzschild) case, that is, $a = 0$, we obtain the elegant result:

$$\ddot{\mathbf{r}} = \frac{-3r_s(L^2+Q)}{2r^5}\mathbf{r} \tag{4.12}$$

where $\mathbf{r} = [x, y, z]$ is the position vector, and $r = ||\mathbf{r}|| = \sqrt{x^2+y^2+z^2}$ is its Euclidean distance from the origin. From the non-rotating ($a = 0$) versions of

equations (4.3) and (4.4) and the conversion equations (4.9), we can write

$$\begin{aligned} L &= x\dot{y} - y\dot{x} \\ Q &= (x\dot{z} - z\dot{x})^2 + (z\dot{y} - y\dot{z})^2. \end{aligned} \tag{4.13}$$

We can now say that $L^2 + Q$ is the square of the impact parameter, which is the perpendicular distance of the initial (straight-line) path of the photon from the point lens. Equation (4.12) is presented in a form similar to the standard Newtonian gravitational equation

$$\ddot{\mathbf{r}} = \frac{-r_s}{2r^3}\mathbf{r}.$$

However, it should be noted that the parameter in equation (4.12) differs in that it includes the time dilation factor, that is, $\dot{t} = r/(r - r_s)$. It will be helpful to explore the Schwarzschild solution in this coordinate system before continuing on to the more general Kerr solution. Expanding equation (4.12) into the three components gives the equality:

$$\frac{\ddot{x}}{x} = \frac{\ddot{y}}{y} = \frac{\ddot{z}}{z},$$

which can be integrated to give the angular momentum conservation equations, analogously with classical mechanics:

$$\begin{aligned} x\dot{y} - y\dot{x} &= L_z \\ x\dot{z} - z\dot{x} &= L_y \\ y\dot{z} - z\dot{y} &= L_x. \end{aligned}$$

In these equations the constants L_x, L_y and L_z are the three components of angular momentum. From equations (4.4) and (4.13), we can identify L with L_z. Taking the inner product of equation (4.12) with $\dot{\mathbf{r}}$ and integrating gives

$$||\dot{\mathbf{r}}||^2 = 1 + \frac{r_s(L^2 + Q)}{r^3},$$

after the integration constant has been determined by the boundary condition $||\dot{\mathbf{r}}|| \to 1$ as $r \to \infty$. Further use of the identity (4.13) enables this to be expressed in the final form

$$(x\dot{x} + y\dot{y} + z\dot{z})^2 = x^2 + y^2 + z^2 - (L_x^2 + L_y^2 + L_z^2) + r_s \frac{L_x^2 + L_y^2 + L_z^2}{\sqrt{x^2 + y^2 + z^2}}. \quad (4.14)$$

Equation (4.14) permits us to identify Q with $L_x^2 + L_y^2$ and we arrive back at the non-rotating version of (4.6). We have identified Q and L in the non-rotating case with the angular momentum of the particle. In the rotating case, we will see that while there are conserved quantities, Q and L, they are not identical with $L_x^2 + L_y^2$ and L_z above. Due to the spherical symmetry of the Schwarzschild system, L and Q only appear in the form $L^2 + Q$. For readability in the Schwarzschild analysis to follow, it is convenient to introduce the non-negative constant $K = L^2 + Q$.

4.3.1 Linearized Schwarzschild Expansion

We can approximate the path taken by photons in the Schwarzschild system, using the expansions:

$$\begin{aligned} x &= X_0 + r_s X_1 + r_s^2 X_2 + O(r_s^3) \\ y &= Y_0 + r_s Y_1 + r_s^2 Y_2 + O(r_s^3) \\ z &= Z_0 + r_s Z_1 + r_s^2 Z_2 + O(r_s^3) \end{aligned} \tag{4.15}$$

where r_s is considered small, relative to the distance of closest approach. Matching terms of corresponding order in r_s will give the zeroth, first and second order solutions. Differentiating the first equation in (4.15) twice and equating with the x-component of equation (4.12) yields:

$$\ddot{X}_0 + r_s \ddot{X}_1 = \frac{-3 r_s x K}{2r^5} + O(r_s^2),$$

where instances of x, y and z in the right side must also be expanded. Matching up the zeroth-order terms gives $\ddot{X}_0 = 0$ (and similarly $\ddot{Y}_0 = 0$ and $\ddot{Z}_0 = 0$). Integrating twice gives us the zeroth order solution

$$\begin{aligned} X_0 &= C_1 \tau + C_2 \\ Y_0 &= C_3 \tau + C_4 \\ Z_0 &= C_5 \tau + C_6 \end{aligned} \tag{4.16}$$

for some constants of integration C_1 to C_6. As is expected, this solution describes a straight line. In order to solve the first-order and second-order equations, it will be necessary to expand r and $K = L^2 + Q$ in powers of r_s using equation (4.15). We write $r = R_0 + r_s R_1 + r_s^2 R_2 + O(r_s^3)$ and then the zeroth order term for r is given by

$$\begin{aligned} R_0^2 &= X_0^2 + Y_0^2 + Z_0^2 \\ &= A\tau^2 + 2B\tau + C \end{aligned}$$

where we have introduced three constants for readability:

$$\begin{aligned} A &= C_1^2 + C_3^2 + C_5^2 \\ B &= C_1 C_2 + C_3 C_4 + C_5 C_6 \\ C &= C_2^2 + C_4^2 + C_6^2. \end{aligned} \tag{4.17}$$

However, we note that in the zeroth order solution, the speed of the massless particle ($= \sqrt{C_1^2 + C_3^2 + C_5^2}$) is 1, so that $A = 1$. The zeroth order term for K is

$$\begin{aligned} K_0 &= (X_0\dot{Y}_0 - Y_0\dot{X}_0)^2 + (X_0\dot{Z}_0 - Z_0\dot{X}_0)^2 + (Z_0\dot{Y}_0 - Y_0\dot{Z}_0)^2 \\ &= C - B^2 \end{aligned}$$

Terms of first order in the small parameter r_s are now equated and we obtain

$$\ddot{X}_1 = \frac{-3X_0K_0}{2R_0^5}.$$

We can now use the substitution $\tau + B = \sqrt{K_0}\tan\gamma$ and integrate twice. This gives the first-order corrections to the light paths

$$\begin{aligned} X_1 &= \frac{X_0}{2R_0} - \frac{R_0}{K_0}(C_2 - BC_1) + C_{11}\tau + C_{21} \\ Y_1 &= \frac{Y_0}{2R_0} - \frac{R_0}{K_0}(C_4 - BC_3) + C_{31}\tau + C_{41} \\ Z_1 &= \frac{Z_0}{2R_0} - \frac{R_0}{K_0}(C_6 - BC_5) + C_{51}\tau + C_{61} \end{aligned} \tag{4.18}$$

Consequently, the first-order velocity components are:

$$\begin{aligned} \dot{X}_1 &= \frac{C_1}{2R_0} - \frac{X_0(\tau + B)}{2R_0^3} - \frac{\tau + B}{R_0K_0}(C_2 - BC_1) + C_{11} \\ \dot{Y}_1 &= \frac{C_3}{2R_0} - \frac{Y_0(\tau + B)}{2R_0^3} - \frac{\tau + B}{R_0K_0}(C_4 - BC_3) + C_{31} \\ \dot{Z}_1 &= \frac{C_5}{2R_0} - \frac{Z_0(\tau + B)}{2R_0^3} - \frac{\tau + B}{R_0K_0}(C_6 - BC_5) + C_{51} \end{aligned} \tag{4.19}$$

Choosing the initial position for the light ray gives us the three constants C_2, C_4 and C_6. We then specify the initial angle of the ray by choosing two of $\dot{x}$, $\dot{y}$ and $\dot{z}$, and the third of these can be identified using the geodesic equations (4.2), (4.3), and (4.4) to determine the speed:

$$\dot{x}^2 + \dot{y}^2 + \dot{z}^2 = \dot{r}^2 + r^2\sin^2\theta\dot{\phi}^2 + r^2\dot{\theta}^2 = 1 + r_sK/r^3. \tag{4.20}$$

This gives the constants C_1, C_3 and C_5. We can then solve for C_{11} to C_{61} in the same way using the equations in (4.18) and (4.19) and the speed equation (4.20). We now have complete path equations for the first order approximation. Converting the velocity given by equations (4.2)-(4.4) (with $a = 0$) to Cartesian co-ordinates gives a constraint on the constants of integration which will be useful

later:

$$C_1C_{11} + C_3C_{31} + C_5C_{51} = 0.$$

4.3.2 Magnification map - binary system

We are now in a position to determine the caustic map due to photons travelling through a system consisting of one or more non-rotating masses, either by tracing their paths using forward integration of equation (4.12) or by solving the first order equations as above. Unsurprisingly, tracing such paths through a system consisting of a central mass and a single planet produces the same diamond caustic pattern, similar to that seen later in the top part of Fig. 4.4, which was described by Wambsganss (1997), and was also plotted previously using 2-dimensional polar co-ordinates in Chapters 2 and 3. Interestingly the computations were slightly quicker with this new Cartesian system, as it was not necessary to rotate each ray into the x, y or r, ϕ plane, and also because the zeroth order terms of $\ddot{x}$, $\ddot{y}$ and $\ddot{z}$ in equation (4.12) are now all zero (whereas those of $\ddot{r}$ and $\ddot{\phi}$ are not). This leaves only small acceleration terms which the numerical integration routine can process more rapidly. Solving the first order equations (4.18), calculated above, gives a caustic map indistinguishable from that obtained using forward integration, but in a much shorter time.

4.3.3 Total Deflection Angle - first order approximation

The well known total deflection for a light ray passing near to a spherically symmetric mass can now easily be estimated to first order in r_s. Due to the spherical symmetry of the space-time around the non-rotating mass, we can choose a ray

FIGURE 4.1: Approximating deflection and delay to the light path near a massive object, located at the origin. For ease of calculations, the light path is chosen so that the ray is horizontal as it crosses the y-axis.

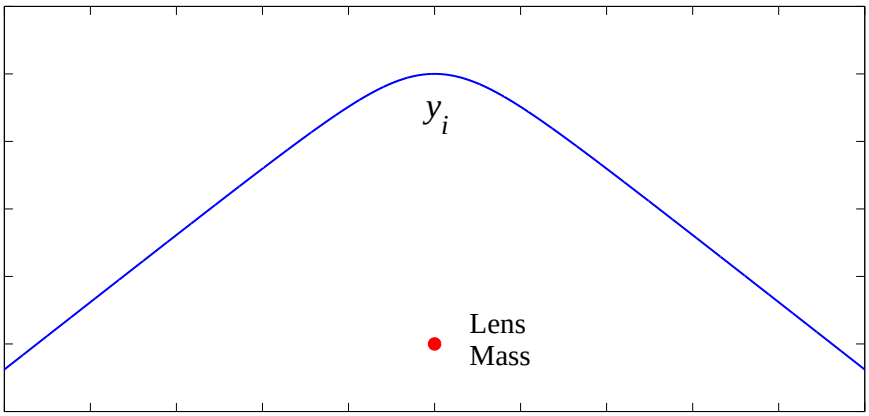

confined to the equatorial plane, without loss of generality. At $\tau = 0$, let the ray cross the y-axis parallel to the x-axis, at some value y_i, as shown in Fig. 4.1. Solving for the speed of the particle at $\tau = 0$, (where $\dot{y} = 0$), it can be seen that $\dot{x}^2 = 1 + r_s K/r^3$. Also, at that point, $x = 0$ and $y = y_i$. It is straightforward to solve for the zeroth-order constants and obtain $C_1 = 1$, $C_2 = 0$, $C_3 = 0$, $C_4 = y_i$. The first-order constants can then be calculated to give $C_{11} = 0$, $C_{21} = 0$, $C_{31} = 0$, $C_{41} = 1/2$. Having the full first-order path equations, the total deflection is given by the difference in $\arctan(\dot{y}/\dot{x})$ as $\tau \to \infty$ and $\arctan(\dot{y}/\dot{x})$ as $\tau \to -\infty$. This gives the result $2r_s/y_i + O(r_s^2)$, which is consistent with the well known Einstein deflection angle. In this case, y_i is the point of closest approach (often referred to as r_0), and also the zeroth-order approximation to the impact parameter, often referred to as b. Thus to first-order in r_s, $2r_s/y_i = 2r_s/b$.

4.3.4 Travel Time Delay - first order approximation

Using the first-order equations again, it is a simple matter to compute the travel-time for a photon from any initial point and time (x_i, y_i, τ_i) to any other point and time (x_f, y_f, τ_f). For ease of computation, and without loss of generality, we may use the same arrangement, and therefore the same constants as described in the angle calculation illustrated in Fig. 4.1 (Section 4.3.3). In order to measure the travel-time to a point of given radius r_f, we solve for τ_f by means of the path equations with the constraint $x_f^2 + y_f^2 = r_f^2$. This will simplify the calculation of the travel time delay for a light ray passing close to the sun. This delay has been calculated to first order previously, and will serve as a check on this new method. We note that y_i is the closest approach to the sun, which is usually designated r_0, Then, at the final point, $\tau = \tau_f$, so $X_0 = \tau_f$ and $Y_0 = r_0$, so that at that point, $R_0 = \sqrt{\tau_f^2 + r_0^2}$. The first order terms are

$$\begin{aligned} X_1 &= \frac{\tau_f}{2\sqrt{\tau_f^2 + r_0^2}} \\ Y_1 &= \frac{r_0}{2\sqrt{\tau_f^2 + r_0^2}} - \frac{\sqrt{\tau_f^2 + r_0^2}}{r_0} + \frac{1}{2}. \end{aligned}$$

To obtain the first-order delay term, we solve for τ_f, and then convert to co-ordinate time t by equation (4.5), giving

$$\begin{aligned} r_f^2 &= x_f^2 + y_f^2 \\ &= \left[\tau_f + \frac{r_s \tau_f}{2\sqrt{\tau_f^2 + r_0^2}}\right]^2 + \left[r_0 + r_s\left(\frac{r_0}{2\sqrt{\tau_f^2 + r_0^2}} - \frac{\sqrt{\tau_f^2 + r_0^2}}{r_0} + \frac{1}{2}\right)\right]^2 + O(r_s^2) \\ &= \tau_f^2 + r_0^2 + r_s(r_0 - \sqrt{\tau_f^2 + r_0^2}) + O(r_s^2). \end{aligned} \tag{4.21}$$

This is a quadratic equation in $\sqrt{\tau_f^2 + r_0^2}$. After solving, we see that

$$\tau_f = \pm\sqrt{r_f^2 - r_0^2}(1 + \frac{r_s}{2(r_f + r_0)}) + O(r_s^2).$$

Solving equation (4.5) to first order and integrating gives $t = \tau + r_s \ln((\tau + R_0)/r_0) + O(r_s^2)$, the constant of integration being determined by letting $t = 0$ when $\tau = 0$. Substituting this into equation (4.21) gives the total travel time

$$t_f = \pm\left(\sqrt{r_f^2 - r_0^2} + \frac{r_s}{2}\sqrt{\frac{r_f - r_0}{r_f + r_0}} + r_s \ln\frac{r_f + \sqrt{r_f^2 - r_0^2}}{r_0}\right) + O(r_s)^2. \quad (4.22)$$

The first term on the right hand side of equation (4.22) is the straight-line time, and the rest constitutes the delay. This delay is in complete agreement with the well known first order delay (for example, see Weinberg (1972) p.202).

4.3.5 Second Order Schwarzschild Expansion

Frame dragging effects due to rotation do not occur at first order, so it will be necessary to consider the Kerr metric equations at second order. Before doing so, it will be worth identifying the second order expansion of the Schwarzschild system. The advantage of this approach is that we can follow the same procedure as above while dealing with fewer terms than in the full rotational model.

The second-order terms X_2, Y_2 and Z_2 in the expansion (4.15) are now considered. First it is necessary to expand $r = \sqrt{x^2 + y^2 + z^2}$ and the constant K to first order in r_s, that is, $r = R_0 + r_s R_1 + O(r_s^2)$ and $K = K_0 + r_s K_1 + O(r_s^2)$. From Section 4.3.1, it is straightforward to establish that

$$\begin{aligned} R_1 &= -\frac{1}{2} + \frac{1}{R_0}(B_R\tau + C_R) \\ K_1 &= 2(C_R - B_R B) \end{aligned}$$

where we have introduced two more constants, B_R and C_R for readability. These are named according to their similarity with the constants B and C in equations (4.17). They are

$$\begin{aligned} B_R &= C_1C_{21} + C_2C_{11} + C_3C_{41} + C_4C_{31} + C_5C_{61} + C_6C_{51} \\ C_R &= C_2C_{21} + C_4C_{41} + C_6C_{61}. \end{aligned}$$

In a manner similar to the first order expansion of Section 4.3.1, we can now expand $\ddot{x}$ to second order, and equation (4.12) yields

$$\ddot{X}_0 + r_s\ddot{X}_1 + r_s^2\ddot{X}_2 = \frac{-3r_s(X_0 + r_sX_1)(K_0 + r_sK_1)}{2(R_0 + r_sR_1)^5} + O(r_s^3).$$

Expanding and matching terms with coefficient r_s^2 gives

$$\begin{aligned} \ddot{X}_2 &= \frac{-3K_0}{2R_0^5}\big(X_1 - 5X_0R_1/R_0 + K_1X_0/K_0\big) \\ &= \frac{-3K_0}{2R_0^5}\left(\frac{3X_0}{R_0} - \frac{R_0}{K_0}(C_2 - BC_1) + C_{11}\tau + C_{21} - \frac{5X_0}{R_0^2}(B_R\tau + C_R) + \frac{K_1}{K_0}X_0\right). \end{aligned}$$

Integrating twice gives the equation for X_2:

$$\begin{aligned} X_2 &= \frac{X_0}{R_0}F_1 + \frac{C_1}{\sqrt{K_0}}F_2 + \frac{C_1 B - C_2}{K_0}F_3 - \frac{C_{21} - C_{11}B}{K_0}R_0 \\ &+ \frac{C_{11}\tau + C_{21}}{2R_0} + C_{12}\tau + C_{22}. \end{aligned} \tag{4.23}$$

The intermediary functions F_1, F_2 and F_3 are given by:

$$\begin{aligned} F_1 &= \frac{9}{16R_0} - \frac{B_R\tau + C_R}{2R_0^2} \\ F_2 &= \frac{B_R R_0}{\sqrt{K_0}} + \frac{9}{16}\arctan\frac{\tau + B}{\sqrt{K_0}} \\ F_3 &= 2R_0\frac{B_R B - C_R}{K_0} + \frac{B_R\tau + C_R}{R_0} + \frac{15}{16}\frac{\tau + B}{\sqrt{K_0}}\arctan\frac{\tau + B}{\sqrt{K_0}} \end{aligned}$$

Due to the spherical symmetry of the Schwarzschild space-time, the equations for Y_2 and Z_2 have a similar form:

$$\begin{aligned} Y_2 &= \frac{Y_0}{R_0}F_1 + \frac{C_3}{\sqrt{K_0}}F_2 + \frac{C_3 B - C_4}{K_0}F_3 - \frac{C_{41} - C_{31}B}{K_0}R_0 \\ &+ \frac{C_{31}\tau + C_{41}}{2R_0} + C_{32}\tau + C_{42} \\ Z_2 &= \frac{Z_0}{R_0}F_1 + \frac{C_5}{\sqrt{K_0}}F_2 + \frac{C_5 B - C_6}{K_0}F_3 - \frac{C_{61} - C_{51}B}{K_0}R_0 \\ &+ \frac{C_{51}\tau + C_{61}}{2R_0} + C_{52}\tau + C_{62} \end{aligned} \tag{4.24}$$

As in Section 4.3.1, we can identify the constants, C_{12}, C_{32} and C_{52} by solving for $\dot{X}_2$, $\dot{Y}_2$ and $\dot{Z}_2$ at $\tau = 0$, and likewise to determine C_{22}, C_{42} and C_{62} we solve for X_2, Y_2 and Z_2 at $\tau = 0$. We can now compare the paths taken by light rays as calculated using the following three methods:

(i) forward integration of equation (4.12);

(ii) zeroth-order path equations (4.16) with first-order corrections (4.18); and

(iii) zeroth-order path equations (4.16) with first-order corrections (4.18) and second-order corrections (4.23) and (4.24).

As the paths within the Schwarzschild system are contained within a plane, we can compare our different solutions in two dimensions without loss of generality. This is illustrated in Fig. 4.2 with $r_s = 0.2$, where the three different methods have been applied to five rays originating from (0,-10) with different starting angles, and each being deflected by the mass at the origin. The three methods agree well in the weak gravity regime at the top of the diagram, and the second order solution does not diverge much from the exact solution until the deflection becomes quite large, that is for rays passing close to the mass.

4.3.6 Deflection angle - second order approximation

Following the earlier procedure for the first order approximation of the total deflection angle in Section 4.3.3, we can now easily determine the second order correction. Of the second order constants, only C_{32} will appear in this calculation, and by noting that $\dot{y} = 0$ at $\tau = 0$, its value is found to be $C_{32} = 0$. The deflection angle is again given by the difference in $\arctan(\dot{y}/\dot{x})$ as $\tau \to \infty$ and $\arctan(\dot{y}/\dot{x})$ as $\tau \to -\infty$. In the system described in Section 4.3.3, and represented in Fig. 4.1, this is approximated by

$$\Delta\Phi \;=\; 2\frac{\dot{y}}{\dot{x}}\bigg|_{\tau\to\infty} = 2\frac{\dot{Y}_0 + r_s\dot{Y}_1 + r_s^2\dot{Y}_2}{\dot{X}_0 + r_s\dot{X}_1 + r_s^2\dot{X}_2}\bigg|_{\tau\to\infty} + O(r_s^3).$$

FIGURE 4.2: Comparison of first and second order path approximations against numerical integration of the full acceleration vector. Rays originate at (-10,0) and are deflected by the mass at (0,0) of Schwarzschild radius 0.2. Five different initial trajectories are chosen, each of which is computed using: forward integration (red); first order approximation (black); second order approximation (blue). In each case, the deflection is greatest with the forward integration of the acceleration vector, and least with the first order path equations.

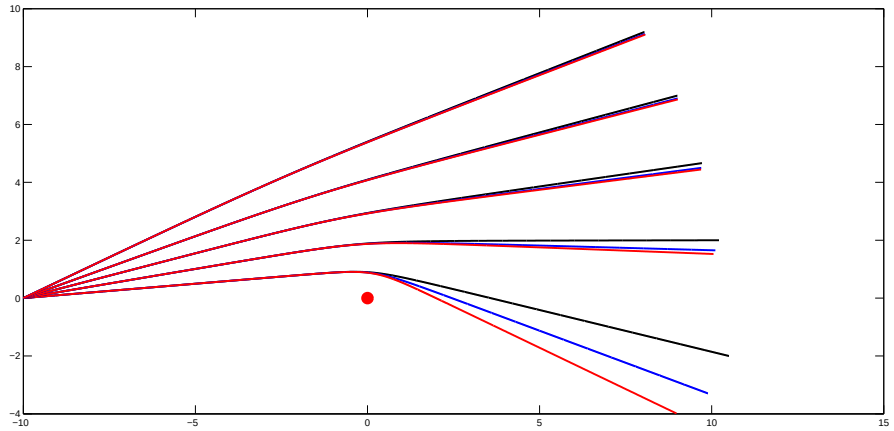

In the system under consideration, $\dot{X}_0 = 1$, $\dot{Y}_0 = 0$ and $\dot{X}_1 \to 0$ as $\tau \to \pm\infty$ so that

$$\begin{aligned}
\Delta\Phi &= 2(r_s\dot{Y}_1 + r_s^2\dot{Y}_2)|_{\tau\to\infty} + O(r_s^3) \\
&= \frac{2r_s}{C_4}\left[1 + \frac{r_s}{2C_4} + \frac{15\pi}{32}\frac{r_s}{C_4}\right] + O(r_s^3) \\
&= \frac{2r_s}{r_0}\left[1 + \frac{r_s}{2r_0} + \frac{15\pi}{32}\frac{r_s}{r_0}\right] + O(r_s^3) \\
&= \frac{2r_s}{b}\left[1 + \frac{15\pi}{32}\frac{r_s}{b}\right] + O(r_s^3)
\end{aligned}$$

where $b = \sqrt{K_0 + r_s K_1} + O(r_s^2) = C_4 + r_s C_4/2 + O(r_s^2)$ is the impact parameter. This deflection to second order is found to be in complete agreement with that calculated by Fishbach & Freeman (1980).

4.3.7 Travel Time Delay - second order approximation

As for the first-order delay calculation, we can calculate the time for the ray to go from r_0 to r_f by solving

$$\begin{aligned} r_f^2 &= x_f^2 + y_f^2 \\ &= X_0^2 + Y_0^2 + 2r_s(X_0X_1 + Y_0Y_1) + r_s^2(X_1^2 + Y_1^2 + 2X_0X_2 + 2Y_0Y_2) \end{aligned}$$

for the time parameter τ_f at the final point. The initial point allows us to calculate the second order constants as $C_{12} = -1/(2r_0^2)$, $C_{22} = 0$, $C_{32} = 0$, $C_{42} = -9/(16r_0)$. Solving for τ_f as in Section 4.3.4, but including terms to second order in r_s gives

$$\begin{aligned} \tau_f &= \sqrt{r_f^2 - r_0^2} + \frac{r_s}{2}\sqrt{\frac{r_f - r_0}{r_f + r_0}} \\ &+ \frac{3r_s^2}{8r_0}\arctan\frac{\sqrt{r_f^2 - r_0^2}}{r_0} - \frac{r_s^2}{8(r_f + r_0)}\sqrt{\frac{r_f - r_0}{r_f + r_0}} + O(r_s^3). \end{aligned} \tag{4.25}$$

Converting from τ to t by integrating equation (4.5), but this time solved to second order, results in

$$t = \tau + r_s \ln\frac{\tau + \sqrt{\tau^2 + r_0^2}}{r_0} + \frac{r_s^2}{2r_0}\left(3\arctan\frac{\tau}{r_0} - \frac{\tau}{\sqrt{\tau^2 + r_0^2}}\right) + O(r_s^3). \tag{4.26}$$

This allows the second order approximation of travel time delay to be written as

$$\begin{aligned} \Delta T &= \frac{r_s}{2}\sqrt{\frac{r_f - r_0}{r_f + r_0}} + r_s \ln\frac{r_f + \sqrt{r_f^2 - r_0^2}}{r_0} \\ &+ r_s^2\left(\frac{15}{8r_0}\arctan\frac{\sqrt{r_f^2 - r_0^2}}{r_0} - \sqrt{\frac{r_f - r_0}{r_f + r_0}}\left(\frac{1}{2r_0} + \frac{1}{8(r_f + r_0)}\right)\right). \end{aligned} \tag{4.27}$$

In order to check this result, we may compare it to the delay (Δt) calculated numerically to high precision using Gaussian quadrature with the formula given in Chapter 2. For a ray starting at earth orbit, grazing the sun ($r_0 = 696000$km and $r_s = 2.95$km) and reaching earth-orbit again, the travel time delay is calculated accurately for a range of orbital distances. In Fig. 4.3 the delay is shown, along with the residuals from the first order and second order approaches. While the first order approximation has a relative error (that is, $(\Delta t - \Delta T)/\Delta t$) of approximately $r_s/r_0 \approx 10^{-6}$, the second order approximation has a relative error of approximately $(r_s/r_0)^2 \approx 10^{-11}$. Distance is shown in astronomical units ('AU'), and time in micro-seconds ('μs').

4.4 Rotating lens

Having explored the Schwarzschild solution in the Cartesian co-ordinate system, we are ready to move on to the rotating (Kerr) case. We may start by adding the rotational terms of the acceleration equations (4.29) which are given in the appendix. These equations can be solved numerically using forward integration to produce a magnification map at the plane containing the observer. As the rotational terms are at second order and greater, the light rays must pass very close to the massive object to make a noticeable change to the trajectory. This is illustrated here by placing the light source close behind the massive lens. In order to observe the change in the pattern, the light source and planet have been placed approximately $3r_s$ away from the black hole, which is clearly not a tenable position for any massive object, but is chosen only to highlight the effect of rotation on the caustic pattern. The top picture in Fig. 4.4 shows the normal diamond caustic without rotation as described by Wambsganss (1997), and calculated here using

FIGURE 4.3: The top picture shows Shapiro delay ("the delay") as calculated using Gaussian Quadrature. The Middle picture shows the difference between the delay and the delay calculated using the first order approximation, and the lower picture shows the difference between the delay and that calculated using the second order approach. The vertical scale is in micro-seconds, the horizontal scale is in astronomical units (AU).

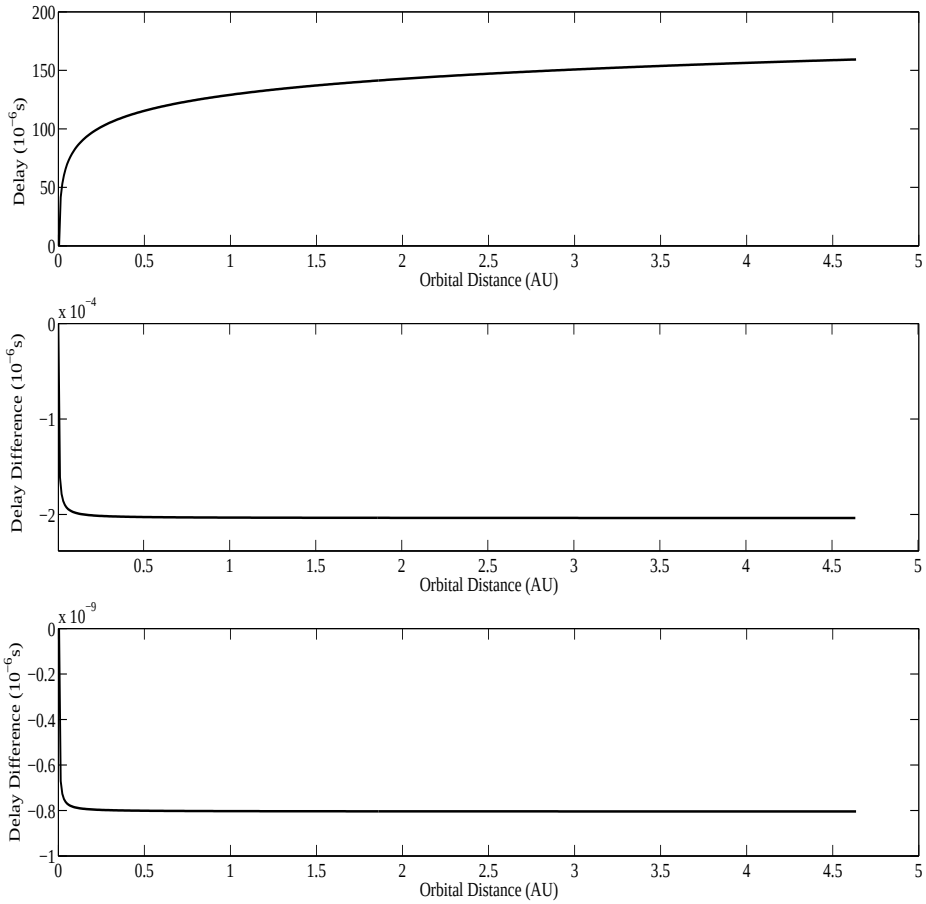

the numerical procedure described in Chapter 2. This was generated using almost 15,000 simulated light rays in a numerical integration of equation (4.12). The lower figure uses the same procedure, but with the addition of the rotational terms. While the diamond caustic pattern is still recognizable, it has clearly undergone a twisting, with the bottom of the shape pushed further over to the right side of the diagram.

4.4.1 Second order Kerr expansion

For a black hole, physically sensible values for the rotational constant a lie between $-r_s/2$ and $+r_s/2$. Therefore it is reasonable to consider a to be of order r_s, that is $a = \alpha r_s$ where α is a constant between $-1/2$ and $1/2$. In the appendix, equation (4.29) has been approximated to second order, resulting in equations (4.30). Expanding the first of these equations using the expansions (4.15), yields

$$\begin{aligned}
\ddot{X}_0 + r_s\ddot{X}_1 + r_s^2\ddot{X}_2 &= \frac{-3r_s(X_0 + r_sX_1)K_0 + r_sK_0)}{2(R_0 + r_sR_1)^5} \\
&+ r_sa\left(\frac{\dot{Y}_0}{R_0^3} + 3(Y_0\dot{Z}_0 - Z_0\dot{Y}_0)\frac{Z_0}{R_0^5} + \frac{Y_0}{R_0^4} + 2\dot{Y}_0\frac{\dot{R}_0}{R_0^3} - 4Y_0\frac{\dot{R}_0^2}{R_0^4}\right) \\
&+ a^2\frac{2\dot{X}_0Z_0}{R_0^5}(2Z_0\dot{R}_0 - R_0\dot{Z}_0) + O(r_s^3).
\end{aligned}$$

In these equations, it can be seen that the first term on the right hand side is the Schwarzschild acceleration discussed in some detail in Section 4.3, which we have already integrated to obtain second-order path equations. It therefore remains to integrate the remaining two terms and to add them to the second-order Schwarzschild solution. The integration is straightforward, and following the same

FIGURE 4.4: Caustic patterns due to central mass and single planet, using forward numerical integration of the full equations (4.12). The top figure has a non-rotating central body, whereas in the bottom diagram the central body is rotating maximally (that is, with $a = r_s/2$). The light source is located on the x-axis at -3×10^{-6}. The primary mass is at the origin with Schwarzschild radius $r_s = 9.9 \times 10^{-7}$, and a planet is located on the z-axis at 3.3×10^{-6} having $r_s = 10^{-8}$. The observer's plane is located at $x = 8000$.

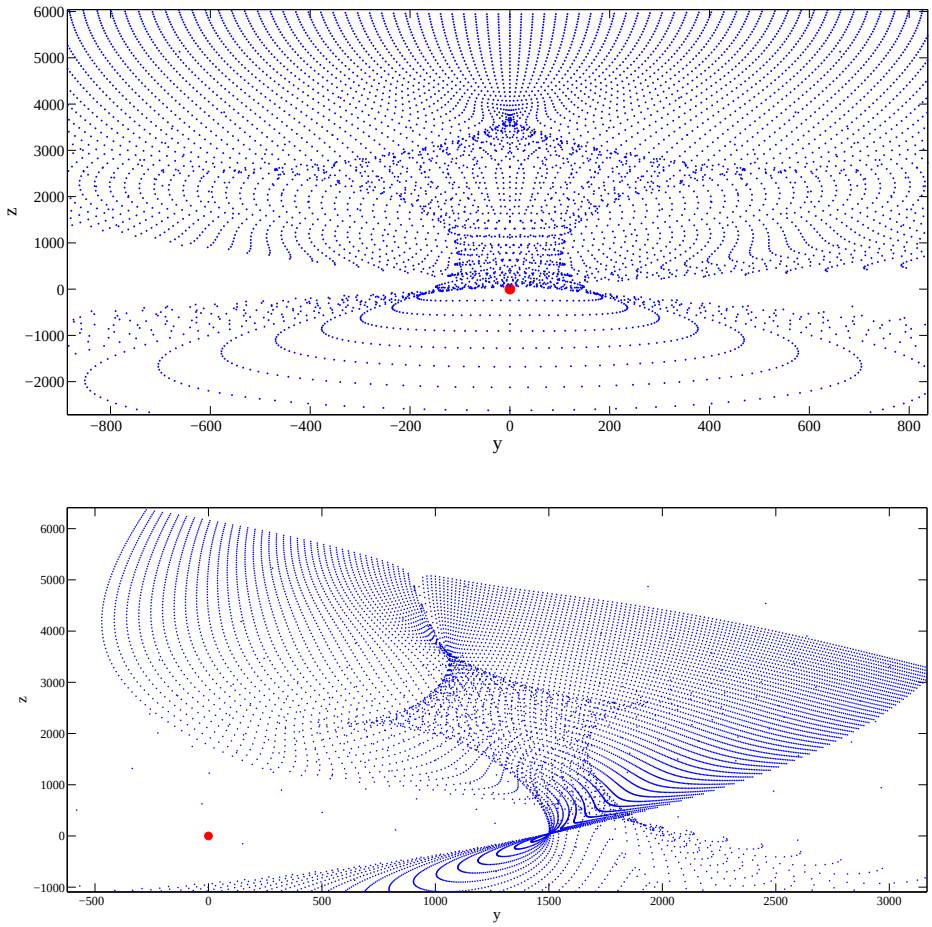

procedure for y and z, we arrive at the second-order path equations.

$$\begin{aligned}
x &= C_1\tau + C_2 + r_s X_1 + r_s^2 X_2 + r_s a\left(L_{x0}F_{RS} + \frac{C_3 R_0}{K_0} - \frac{Y_0}{2R_0^2}\right) - a^2 C_1 F_A + O(r_s^3) \\
y &= C_3\tau + C_4 + r_s Y_1 + r_s^2 Y_2 + r_s a\left(L_{y0}F_{RS} - \frac{C_1 R_0}{K_0} + \frac{X_0}{2R_0^2}\right) - a^2 C_3 F_A + O(r_s^3) \\
z &= C_5\tau + C_6 + r_s Z_1 + r_s^2 Z_2 + r_s a L_{z0} F_{RS} - a^2 C_5 F_A + O(r_s^3)
\end{aligned}$$

in which X_1, Y_1, Z_1 and X_2, Y_2, Z_2 are described in Sections 4.3.1 and 4.3.5. The remaining terms are

$$\begin{aligned}
F_{RS} &= 2R_0\frac{C_6 - BC_5}{K_0^2} - \frac{Z_0}{R_0 K_0} \\
F_A &= \frac{Q_0(\tau + B) - 2C_5 K_0 Z_0}{2R_0^2 K_0} + \frac{Q_0}{2K_0^{3/2}} \arctan\frac{\tau + b}{\sqrt{K_0}} \\
L_{x0} &= C_4 C_5 - C_3 C_6 \\
L_{y0} &= C_2 C_5 - C_1 C_6 \\
L_{z0} &= C_2 C_3 - C_1 C_4 \\
Q_0 &= L_{x0}^2 + L_{y0}^2.
\end{aligned}$$

In order to estimate travel-time delays, as above we write co-ordinate time t as a function of τ. Expanding $\dot{t}$ to second order in r_s, and integrating yields

$$\begin{aligned}
t &= \tau + r_s \log\left(\frac{\tau + B + R_0}{B + \sqrt{C}}\right) + \frac{\frac{3}{2}r_s^2 + a^2}{\sqrt{K_0}} \arctan\frac{\tau\sqrt{K_0}}{B\tau + C} \\
&- r_s\tau\frac{r_s(B_R B - C_R) + aL_{z0}}{K_0 R_0} + O(r_s^3).
\end{aligned}$$

Again, the constants of integration have been determined by setting $t = 0$ when $\tau = 0$.

4.4.2 Second order expansion - equatorial case

It is clear that in the equatorial case ($z = \dot{z} = 0$, which also means that $C_5 = C_6 = Q_0 = L_{x0} = L_{y0} = 0$ and $K_0 = L_{z0}^2$) the above equations simplify to

$$\begin{aligned} x &= C_1\tau + C_2 + r_s X_1 + r_s^2 X_2 + r_s a\left(\frac{C_3 R_0}{L_{z0}^2} - \frac{Y_0}{2R_0^2}\right) + O(r_s^3) \\ y &= C_3\tau + C_4 + r_s Y_1 + r_s^2 Y_2 - r_s a\left(\frac{C_1 R_0}{L_{z0}^2} - \frac{X_0}{2R_0^2}\right) + O(r_s^3) \end{aligned}$$

Interestingly, while terms involving r_s^2, $r_s a$ and a^2 are all of second order in the expansion parameter, and terms with coefficients r_s^2 and $r_s a$ appear in these equatorial equations, there are no such terms with coefficient a^2.

4.4.3 Total Deflection angle - second order equatorial Kerr approximation

We can now add the second order term due to rotation to the earlier total deflection angle calculation. As for the earlier scenario (see Fig. 4.1), $C_1 = 1$ and $C_3 = 0$ so that as τ goes to $\pm\infty$, $R_0 \to \infty$, and so $\dot{y} \to r_s\dot{Y}_1 + r_s^2\dot{Y}_2 - r_s a\tau/(R_0 L_{z0}^2)$. Then the deflection becomes

$$\begin{aligned} \Delta\Phi &= 2\left(r_s\dot{Y}_1 + r_s^2\dot{Y}_2 - r_s a\frac{1}{L_{z0}^2}\right)\Bigg|_{\tau\to\infty} + O(r_s^3) \\ &= \frac{2r_s}{r_0}\left(1 + \frac{r_s}{2r_0} + \frac{15\pi}{32}\frac{r_s}{r_0} - \frac{a}{r_0}\right) + O(r_s^3) \\ &= \frac{2r_s}{b}\left(1 + \frac{15\pi}{32}\frac{r_s}{b} - \frac{a}{b}\right) + O(r_s^3). \end{aligned}$$

This deflection is found to be in complete agreement with that calculated by Edery & Godlin (2006).

4.4.4 Travel Time Delay - second order equatorial Kerr approximation

As before, but including the rotational components of x and y, the travel time for the ray to go from r_0 to r_f can be calculated by solving

$$\begin{aligned} r_f^2 &= x_f^2 + y_f^2 \\ &= X_0^2 + Y_0^2 + 2r_s(X_0X_1 + Y_0Y_1) + r_s^2(X_1^2 + Y_1^2 + 2X_0X_2 + 2Y_0Y_2) \\ &+ r_s a\left(X_0(\frac{C_3R_0}{L_{z0}^2} - \frac{Y_0}{2R_0^2}) - Y_0(\frac{C_1R_0}{L_{z0}^2} - \frac{X_0}{2R_0^2})\right) + O(r_s^3) \\ &= X_0^2 + Y_0^2 + 2r_s(X_0X_1 + Y_0Y_1) + r_s^2(X_1^2 + Y_1^2 + 2X_0X_2 + 2Y_0Y_2) \\ &+ r_s a\frac{R_0}{L_{z0}} + O(r_s^3) \end{aligned} \tag{4.28}$$

for the overall time τ_f. As previously, the initial point allows us to calculate the second order constants. With rotation these constants become $C_{12} = -1/(2r_0^2)$, $C_{22} = a/(2r_sr_0)$, $C_{32} = -a/(2r_sr_0^2)$, $C_{42} = a/(r_sr_0) - 9/(16r_0)$. The solution for τ_f now includes a rotational term (dependent on a), and becomes

$$\begin{aligned} \tau_f &= \sqrt{r_f^2 - r_0^2} + \frac{r_s}{2}\sqrt{\frac{r_f - r_0}{r_f + r_0}} + \frac{3r_s^2}{8r_0}\arctan\frac{\sqrt{r_f^2 - r_0^2}}{r_0} \\ &- \frac{r_s^2}{8(r_f + r_0)}\sqrt{\frac{r_f - r_0}{r_f + r_0}} + \frac{r_s a}{r_0}\sqrt{\frac{r_f - r_0}{r_f + r_0}} + O(r_s^3). \end{aligned}$$

The conversion from τ to t also now includes rotational terms

$$t = \tau + r_s\ln\frac{\tau + \sqrt{\tau^2 + r_0^2}}{r_0} + \frac{3r_s^2 + 2a^2}{2r_0}\arctan\frac{\tau}{r_0} + r_s\tau\frac{2a - r_s}{r_0\sqrt{\tau^2 + r_0^2}} + O(r_s^3).$$

This allows us to write the second order approximation of travel time delay as

$$\begin{aligned}\Delta T &= \frac{r_s}{2}\sqrt{\frac{r_f - r_0}{r_f + r_0}} + r_s \ln \frac{r_f + \sqrt{r_f^2 - r_0^2}}{r_0} + \left(\frac{15r_s^2}{8r_0} + \frac{a^2}{r_0}\right) \arctan \frac{\sqrt{r_f^2 - r_0^2}}{r_0} \\ &+ r_s\sqrt{\frac{r_f - r_0}{r_f + r_0}}\left(\frac{a}{r_f} + \frac{4a - r_s}{2r_0} - \frac{r_s}{8(r_f + r_0)}\right).\end{aligned}$$

This delay is the same for a ray travelling from perihelion r_0 to r_f on the right (t positive) as for a ray travelling from r_f on the left (t negative) to r_0. So the total delay for a ray passing the massive object at the origin is twice the amount ΔT stated above. It can be seen in this example, that if a is positive (that is, the mass has anti-clockwise angular momentum), the motion of the particle is opposite to the frame-dragging effects, and the travel time delay is increased. Conversely, if a is negative the travel time delay is decreased. Dymnikova (1986) has calculated the delay to second order in the limit $r_f >> r_0$. The delay given here in the last equation is in agreement with Dymnikova's result in the same limit, but it also gives the second order delay for all values of r_f.

4.5 Modelling delay for a binary pulsar system

The regularity of pulses from a millisecond pulsar provides an interesting possibility for observing the effect of rotation on the travel time of the light pulses. A system such as the double pulsar binary system J0737-3039 described by Burgay et al. (2003) may provide interesting possibilities for observing the delay due to a rapidly rotating massive object. We will construct a simpler mathematical model by replacing one of the pulsars in that system with a black hole (with rotation also in the same plane as the orbit and observer) so that there is confidence in using

the Kerr metric equations. Thus we consider here a binary system consisting of a millisecond pulsar and a rotating black hole with the orbital plane aligned so that the observer and the two bodies are within the same plane. We also ignore any atmospheric or magnetospheric interference which may introduce complications in measurements in the real system mentioned above. Finally we will ignore the modulation of the pulse timing due to the spinning of the pulsar. This last effect is expected to be small for a millisecond pulsar with an orbital period of hours or days, such as we are considering.

Additionally, it must be pointed out that in this simulation, we are ignoring the effect of the mass of the pulsar on the trajectory and travel-time of the light rays. Any effect on the travel-time for photons climbing out of the pulsar's gravity well would be expected to be the same for every photon, and as the photons are emitted radially there would be no initial effect on the trajectory. However, this system is actually a two body system, so there will be some effect, however small, due to the mass of the pulsar, which is not quantified in the present work.

Having designed this system with the orbital plane and the observer in the equatorial plane of the black hole, we can use the simpler two dimensional equatorial equations of Section 4.4.2 to describe the paths of light rays from the pulsar to the observer. This is for simplicity and clarity only; another arrangement using the full three dimensional equations is only slightly more difficult to describe and to code. In order to determine the delay of pulses due to the rotating black hole, we will send light rays back from the observer past the black hole using forward integration of the equatorial equations, stopping the integration procedure when the rays meet the orbital distance of the pulsar. As the time coordinate has been reversed, note that this also entails reversing the direction of spin of the black hole

(which is decided arbitrarily in this model, but should be considered when using data from a real system).

Fig. 4.5 shows the last section of rays as they reach the circular orbit of the pulsar. Due to the large difference between the vertical and horizontal scales, and because only a small section of the orbit is shown, the endpoints of the rays appear to be in a line, but they do in fact form a circular arc. All distances shown are in light-seconds and times for the delays are in seconds. The Schwarzschild radius (r_s) of the black hole is 2×10^{-4} light-seconds, equivalent to approximately 20 solar masses. The delay increases in an almost linear relationship with mass of the lens, so that a black hole of 10 solar masses would have approximately half the delay times as those shown in Fig. 4.6. In a different study of travel time delay in a binary pulsar system, Laguna & Wolszczan (1997) note that in order for the binary system to have sufficient longevity for a reasonable chance of observation, there are limitations on the proximity of the pulsar to the black hole, with approximately 5 solar radii being near optimum compromise between longevity and magnitude of the delay effect. We therefore place the circular orbit at 11.6 light-seconds, approximately 5 solar radii. This orbit induces a delay term in the straight-line time from -11.6 seconds when the pulsar is closest to the observer, to $+11.6$ seconds when it is furthest from the observer. However, in the present study, we are interested in the additional asymmetric delay due to rotation. The orbital delay is symmetric about the point of superior conjunction, or occultation, which occurs when the lensing body is directly between the pulsar and the observer. For this reason, the orbital delay will be ignored here.

Along with the equatorial equations, we also integrate equation (4.5) to keep track of the time coordinate. Comparing the time taken with the time light would take to travel in a straight line from pulsar to observer without any lensing object

FIGURE 4.5: Rays from observer to pulsar orbit at radius of 11.6 light-seconds, using forward integration past a maximally rotating central body ($r_s = 2 \times 10^{-4}$). Only the final sections of the rays are shown. Rays passing very close to the mass, and experiencing large deflection, are not shown here because the images produced by such rays are extremely faint.

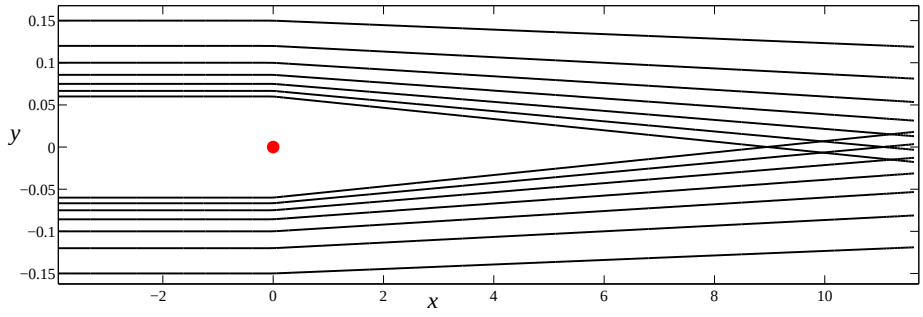

gives the delay, shown in Fig. 4.6. The solid curve represents the delay due to a rotating black hole, and was calculated using forward integration of the equatorial equations (4.31) given in the appendix. This delay is plotted against the angle from superior conjunction. That is, a zero angle represents the system with the black hole in between the pulsar and observer, while all three are in a line. The dashed line represents the delay due to a non-rotating black hole, calculated using the Schwarzschild acceleration, equation (4.12). The part of the delay due to rotation is small, and so to highlight the difference between the delays shown, a magnified portion near the intersection is shown in the lower figure.

Finally the delay due to maximal rotation of the black hole is subtracted from the delay due to a black hole of the same mass without rotation. The difference between these delays gives the delay due solely to rotation, which provides a small asymmetry in the delay curve in the rotational case. This difference is shown in Fig. 4.7. The upper and lower lines represent the delay difference for the two different images of the source, one passing to the left of the mass, the other to the

FIGURE 4.6: Delay due to black hole. Four curves are present for rays passing on each side of the black hole, and in the cases where the black hole is rotating (solid lines) or not rotating (dashed lines). The change in delay due to rotation is small so the curves in each pair are very close together. The lower figure shows a magnification of the central section, which allows the different delays to be seen.

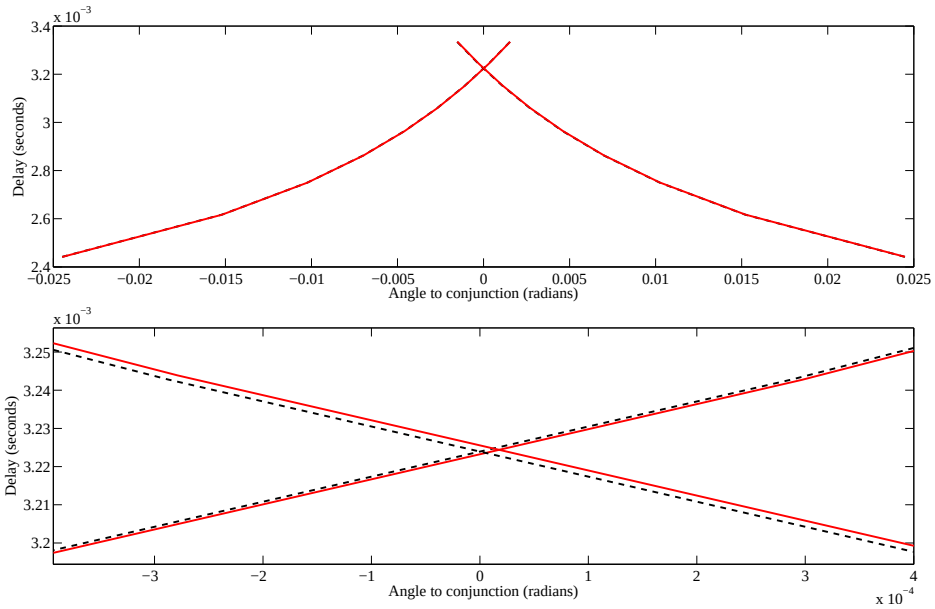

right. One of these images is dominant prior to conjunction, and the other image becomes dominant after conjunction.

The delays due to lensing in this system are of the order of 10^{-3} seconds, while the asymmetric part of the delay that is due to rotation is of the order of 10^{-6} seconds. Assuming other effects on travel time can be adequately accounted for, these rotational delays may be measurable, and could possibly be used to estimate the angular momentum of the lens.

FIGURE 4.7: Difference in travel-time delay between rotating and non-rotating cases, plotted against orbital position of the pulsar. Each curve corresponds to rays passing the black hole on either the left (opposed to the black hole's rotation) or right side (aligned to the rotation).

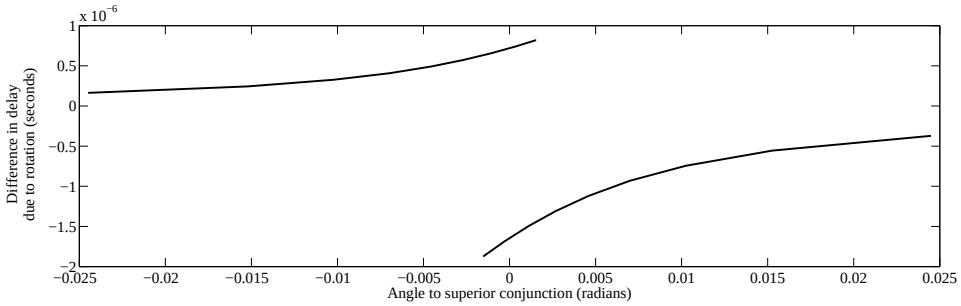

4.6 Conclusion and Discussion

In this chapter, we have presented Cartesian acceleration components for photons using the Kerr metric. While these components are somewhat complicated, they allow easy modelling of systems in Cartesian coordinates, with the advantage that the components are normally very small. This allows for rapid numerical integration, and a new result (the caustic shape due to a binary system with rotating mass) has been presented. In order to approximate the light paths near a rotating black hole, we have built up the approximations in stages, beginning with the zeroth order and first order expansions, followed by the second order Schwarzschild expansion and finally the second order Kerr expansion. At each point, the versatility of this approach has been demonstrated by the ease of calculating deflection and travel time delay, which are found to match previously calculated amounts. In addition, a new formula for delay due to spinning black holes was presented. It may prove possible in some practical astrophysical circumstances to measure directly the delay due to rotation of the lensing object, and so to infer the angular

momentum, using the formulae presented here. This awaits future experimental observation.

4.7 Appendix to Chapter 4

In this appendix, the Cartesian acceleration components are written out in full. The dot denotes differentiation by the chosen parameter τ. These equations are followed by their second order approximations. Next the x and y acceleration components for the equatorial special case are presented, followed by their second order approximations.

4.7.1 Three-Dimensional Acceleration Components

Expanding and simplifying equation (4.10) for $\ddot{x}$ and following the same procedure for $\ddot{y}$ and $\ddot{z}$, we can derive the following forms of the acceleration components:

$$\begin{aligned}
\ddot{x} &= -\frac{3r_s x}{2r^3}\frac{Q+(L-a)^2}{r^2+a^2} - \frac{a^2\dot{r}\dot{x}}{r}\left(\frac{1}{a^2+r^2}+\frac{z^4}{r^2(r^2-z^2)^2}\right) + \frac{ax}{r^2+a^2}G_1 + \frac{ay}{\Delta}G_2 \\
\ddot{y} &= -\frac{3r_s y}{2r^3}\frac{Q+(L-a)^2}{r^2+a^2} - \frac{a^2\dot{r}\dot{y}}{r}\left(\frac{1}{a^2+r^2}+\frac{z^4}{r^2(r^2-z^2)^2}\right) + \frac{ay}{r^2+a^2}G_1 - \frac{ax}{\Delta}G_2 \\
\ddot{z} &= -\frac{3r_s z(Q+(L-a)^2)}{2r^5} + \frac{2a^2 z(Q-z^2)}{r^6}.
\end{aligned} \tag{4.29}$$

The functions G_1 and G_2 are functions of $x, y, z, \dot{x}, \dot{y}, \dot{z}$ and are of order r_s. The axi-symmetry of the system may be seen in the signs in the equations for $\ddot{x}$ and $\ddot{y}$. That is, the equations are invariant under a rotation of the system about the

z-axis such as given by the transformations $x \to y, y \to -x$. The functions G_1 and G_2 are expressed below:

$$
\begin{aligned}
G_1 &= a\dot{r}^2\left(\frac{2}{a^2+r^2}+\frac{z^4(a^2z^2+r^4)}{r^4(r^2-z^2)^3}-\frac{z^2}{r^2(r^2-z^2)}\right)+\frac{az\dot{r}\dot{z}(r^6-a^2z^4-2r^4z^2)}{r^3(r^2-z^2)^3}\\
&- \frac{a}{r^6}(2a^2z^2+r^4+2r^2z^2)+\frac{aL^2}{r^4}\left(\frac{r^2+z^2}{r^2-z^2}+\frac{2r^3r_s}{\Delta(r^2-z^2)}-\frac{a^2(a^2+r^2)}{\Delta^2}\right)\\
&- \frac{r_s}{r\Delta}\big(a^2+r^2-r^2\dot{r}\big)\left[2L\left(\frac{1}{r^2-z^2}-\frac{a^2}{\Delta r^2}\right)+a\frac{r_s}{r\Delta}\left(1-\frac{r^2\dot{r}}{a^2+r^2}\right)\right]+\frac{aQ}{r^4}\\
G_2 &= r_s\frac{2r^2(Q+L^2-a^2)+4a^2Q-3rr_s(Q+(L-a)^2)}{2r^4(a^2+r^2)}\\
&+ \frac{2z(z\dot{r}-r\dot{z})}{r^3(r^2-z^2)}\left(\frac{r^3r_s\dot{r}}{a^2+r^2}+aL-rr_s\right)\\
&+ \frac{r_s\dot{r}^2}{a^2+r^2}\left(\frac{a^2-r^2}{\Delta}+\frac{2a^2}{a^2+r^2}\right)-\frac{\dot{r}}{r^2\Delta}\big(r_s(a^2-r^2)+aL(2r-r_s)\big)\\
&+ \frac{a\dot{r}}{r^2}\left(\frac{r^2-2z^2}{(r^2-z^2)^2}-\frac{a^2}{r^2(a^2+r^2)}\right)\left(r_sa+\frac{\Delta Lr}{r^2-z^2}-\frac{a^2L}{r}-\frac{ar^2r_s\dot{r}}{a^2+r^2}\right)
\end{aligned}
$$

The constants of motion L and Q and also r and Δ can be expressed as the following functions of $x, y, z, \dot{x}, \dot{y}, \dot{z}$:

$$
\begin{aligned}
r &= \sqrt{\frac{x^2+y^2+z^2-a^2+\sqrt{(x^2+y^2+z^2-a^2)^2+4a^2z^2}}{2}}\\
L &= \frac{r(r^2-z^2)}{r^4-r_sr^3+a^2z^2}\left(r\Delta\frac{x\dot{y}-y\dot{x}}{x^2+y^2}-r_sa(1-\frac{r^2\dot{r}}{a^2+r^2})\right)\\
Q &= \frac{r^2(z\dot{r}-r\dot{z})^2+L^2z^2}{r^2-z^2}-\frac{a^2z^2}{r^2}\\
\Delta &= a^2+r^2-r_sr
\end{aligned}
$$

4.7.2 Second Order Approximation

In order to approximate $\ddot{x}, \ddot{y}$ and $\ddot{z}$ to second order in r_s, it is only necessary to approximate G_1 and G_2 to first order in r_s, as they are multiplied by a, which is of order r_s. We first express the intermediary functions to first order in r_s. Ignoring terms of second order and higher in r_s, where a is of order r_s, we have the following simplifications:

$$\begin{aligned} L &= L_z + O(r_s^2) = x\dot{y} - y\dot{x} + O(r_s^2) \\ r &= \sqrt{x^2+y^2+z^2} + O(r_s^2) \\ Q &= L_x^2 + L_y^2 + O(r_s^2) = (y\dot{z} - z\dot{y})^2 + (x\dot{z} - z\dot{x})^2 + O(r_s^2) \\ \Delta &= r^2 - r_s r + O(r_s^2) \end{aligned}$$

So that G_1 and G_2 can be approximated by:

$$\begin{aligned} G_1 &= a\dot{r}^2\left(\frac{2}{r^2} + \frac{z^4}{(r^2-z^2)^3} - \frac{z^2}{r^2(r^2-z^2)}\right) + \frac{ar\dot{r}z\dot{z}(r^2-2z^2)}{(r^2-z^2)^3} + \frac{2r_sL}{r}\frac{\dot{r}-1}{r^2-z^2} \\ &+ \frac{a}{r^4}\left(Q + L^2\frac{r^2+z^2}{r^2-z^2} - r^2 - 2z^2\right) \\ G_2 &= \frac{r_s(Q+L^2)}{r^4} + \frac{2z(z\dot{r} - r\dot{z})}{r^3(r^2-z^2)}\left(rr_s(\dot{r}-1) + aL\right) - \frac{r_s\dot{r}}{r^2}(\dot{r}-1) \\ &- 2aL\frac{\dot{r}}{r^3} + aLr\dot{r}\frac{r^2-2z^2}{(r^2-z^2)^3} \end{aligned}$$

We can then write the acceleration components, $\ddot{x}, \ddot{y}, \ddot{z}$ as:

$$\begin{aligned}
\ddot{x} &= -\frac{3r_s x}{2r^5}(Q + L^2 - 2aL) - \frac{a^2 \dot{r}\dot{x}}{r^3}\left(1 + \frac{z^4}{(r^2 - z^2)^2}\right) + \frac{ax}{r^2}G_1 + \frac{ay}{r^2}G_2 + O(r_s^3) \\
\ddot{y} &= -\frac{3r_s y}{2r^5}(Q + L^2 - 2aL) - \frac{a^2 \dot{r}\dot{y}}{r^3}\left(1 + \frac{z^4}{(r^2 - z^2)^2}\right) + \frac{ay}{r^2}G_1 - \frac{ax}{r^2}G_2 + O(r_s^3) \\
\ddot{z} &= -\frac{3r_s z(Q + L^2 - 2aL)}{2r^5} + \frac{2a^2 z(Q - z^2)}{r^6} + O(r_s^3)
\end{aligned}$$

After some algebra, these may be written as:

$$\begin{aligned}
\ddot{x} &= -\frac{3r_s x}{2r^5}(Q + L^2) + r_s a\left(\frac{\dot{y}}{r^3} + 3(y\dot{z} - z\dot{y})\frac{z}{r^5} + \frac{y}{r^4} + 2\dot{y}\frac{\dot{r}}{r^3} - 4y\frac{\dot{r}^2}{r^4}\right) \\
&- a^2\frac{2\dot{x}z}{r^5}(2z\dot{r} - r\dot{z}) + O(r_s^3) \\
\ddot{y} &= -\frac{3r_s y}{2r^5}(Q + L^2) - r_s a\left(\frac{\dot{x}}{r^3} + 3(x\dot{z} - z\dot{x})\frac{z}{r^5} + \frac{x}{r^4} + 2\dot{x}\frac{\dot{r}}{r^3} - 4x\frac{\dot{r}^2}{r^4}\right) \\
&- a^2\frac{2\dot{y}z}{r^5}(2z\dot{r} - r\dot{z}) + O(r_s^3) \\
\ddot{z} &= -\frac{3r_s z}{2r^5}(Q + L^2) - r_s a\frac{3Lz}{r^5} + a^2\frac{2z(Q - z^2)}{r^6} + O(r_s^3)
\end{aligned} \tag{4.30}$$

4.7.3 Equatorial Equations

From equation (4.29), we can see that a particle in the $x-y$ plane has no component of acceleration in the z direction. That is, if $z = 0$, then $\ddot{z} = 0$. If such a particle also has no velocity component in the z direction it must remain within the plane. Thus there is a 2-D special case. The equations are derived by setting z and $\dot{z}$ to zero. This also means that Q is zero. Then we have the following acceleration components:

$$\ddot{x} = -\frac{3r_s x}{2r^3}\frac{(L-a)^2}{r^2+a^2} - \frac{a^2\dot{r}\dot{x}}{r}\frac{1}{a^2+r^2} + \frac{ax}{r^2+a^2}G_1 + \frac{ay}{\Delta}G_2$$
$$\ddot{y} = -\frac{3r_s y}{2r^3}\frac{(L-a)^2}{r^2+a^2} - \frac{a^2\dot{r}\dot{y}}{r}\frac{1}{a^2+r^2} + \frac{ay}{r^2+a^2}G_1 - \frac{ax}{\Delta}G_2 \qquad (4.31)$$

where G_1 and G_2 are now given by:

$$\begin{aligned} G_1 &= a\dot{r}^2\left(\frac{2}{a^2+r^2}\right) - \frac{a}{r^2} + \frac{aL^2}{r^4}\left(1 + \frac{2rr_s}{\Delta} - \frac{a^2(a^2+r^2)}{\Delta^2}\right) \\ &- \frac{r_s}{r\Delta}\left(a^2+r^2-r^2\dot{r}\right)\left[\frac{2L}{r^2}\left(1-\frac{a^2}{\Delta}\right) + \frac{r_s a}{r\Delta}\left(1 - \frac{r^2\dot{r}}{a^2+r^2}\right)\right] \\ G_2 &= \frac{r_s}{a^2+r^2}\left[\dot{r}^2\left(\frac{a^2}{a^2+r^2} + \frac{a^2-r^2}{\Delta}\right) + \frac{2r(L^2-a^2) - 3r_s(L-a)^2}{2r^3}\right. \\ &- \left.\frac{\dot{r}}{r\Delta}(aL(r-r_s) + r_s a^2)\right] + \frac{\dot{r}}{r\Delta}(r_s r - aL). \end{aligned}$$

Here, r, $\dot{r}$ and L are given by

$$\begin{aligned} r^2 &= x^2 + y^2 - a^2 \\ \dot{r} &= \frac{x\dot{x} + y\dot{y}}{r} \\ L &= \frac{1}{r-r_s}\left(r\Delta\frac{x\dot{y} - y\dot{x}}{x^2+y^2} - r_s a(1 - \frac{r^2\dot{r}}{a^2+r^2})\right). \end{aligned}$$

4.7.4 Equatorial Case: Second Order Approximation

Discarding terms of order higher than r_s^2 (where again, a is of order r_s), we obtain the following acceleration components:

$$\ddot{x} = -\frac{3r_s x}{2r^5}(L^2 - 2aL) - \frac{a^2\dot{r}\dot{x}}{r^3} + \frac{ax}{r^2}G_1 + \frac{ay}{r^2}G_2$$
$$\ddot{y} = -\frac{3r_s y}{2r^5}(L^2 - 2aL) - \frac{a^2\dot{r}\dot{y}}{r^3} + \frac{ay}{r^2}G_1 - \frac{ax}{r^2}G_2$$

where G_1 and G_2 are now given by:

$$\begin{aligned} G_1 &= a\dot{r}^2\left(\frac{2}{r^2}\right) - \frac{a}{r^2} + \frac{aL^2}{r^4} - \frac{2r_sL}{r^3}(1-\dot{r}) \\ G_2 &= \frac{r_s\dot{r}}{r^2}\left[1 - \dot{r} + \frac{L^2}{r^2}\right] - \frac{aL\dot{r}}{r^3}. \end{aligned}$$

In these expressions, r, $\dot{r}$ and L are given by

$$\begin{aligned} r^2 &= x^2 + y^2 \\ \dot{r} &= \frac{x\dot{x} + y\dot{y}}{r} \\ L &= L_z + O(r_s^2) = x\dot{y} - y\dot{x} + O(r_s^2) \end{aligned}$$

After some algebra, in which all the terms associated with a^2 cancel out, $\ddot{x}$ and $\ddot{y}$ may be written as:

$$\begin{aligned} \ddot{x} &= -\frac{3r_sx}{2r^5}L^2 + r_sa\left(\frac{\dot{y}}{r^3} + \frac{y}{r^4} + 2\dot{y}\frac{\dot{r}}{r^3} - 4y\frac{\dot{r}^2}{r^4}\right) + O(r_s^3) \\ \ddot{y} &= -\frac{3r_sy}{2r^5}L^2 - r_sa\left(\frac{\dot{x}}{r^3} + \frac{x}{r^4} + 2\dot{x}\frac{\dot{r}}{r^3} - 4x\frac{\dot{r}^2}{r^4}\right) + O(r_s^3) \end{aligned} \qquad (4.32)$$

Chapter 5

Conclusion

This work has presented an alternative approach to identifying the path a photon should travel in proximity to massive objects. The study began with the simplest non-trivial solution to Einstein's equations of General Relativity, the Schwarzschild metric. A simple formula was written which allowed the total deflection to the path of a photon passing near a spherically symmetric body, to be computed numerically to arbitrary accuracy. Next an effective refractive index was developed which accurately describes the effect of space-time on the photon's path. This refractive index was used to write a new and simple integral for the travel-time delay ('Shapiro delay'), allowing the delay to be computed to arbitrary accuracy.

A new acceleration vector in plane polar co-ordinates was identified which accurately describes the path of a photon in a Schwarzschild space-time. It was shown that the well known radius for circular orbit for a photon is an obvious outcome of this acceleration vector. Using this acceleration vector, a kinematic system of equations was used to model numerically the path of a photon passing close to the sun. The values for deflection and delay thus derived were found to match

those previously calculated. Making the approximation that the total acceleration on the photon is the sum of the individual acceleration vectors due to each mass, light paths through systems containing two bodies were modelled. This resulted in the diamond caustic patterns expected for such binary systems, demonstrating the versatility of this new approach.

A formal linearisation for the light path in a Schwarzschild space-time was developed in Chapter 3. Starting with the acceleration vector described in Chapter 2, a perturbation expansion about a straight line was performed, using an appropriate small parameter. This resulted in a third-order differential equation, surprisingly yielding a closed-form solution. This allowed the path of the photon to be described, accurate to first order in the small parameter. It was shown that this solution matches the simplest first order solution in the limit of large source-to-lens and observer-to-lens distances. As this solution was linear, the superposition principle allows calculation of deflection due to multiple masses, simply by summing the small perturbations due to each mass. In this way, caustic maps were produced, which are indistinguishable from both the simplest first order approach, as well as from the figure produced by integration of the acceleration vectors as in Chapter 2.

The effect of the rotation of massive objects upon light rays was considered in Chapter 4. Beginning with the Kerr metric, the acceleration components were identified. Due to the fully three-dimensional nature of the path of light through a Kerr space-time, Cartesian co-ordinates were chosen. This meant that all zeroth order components of acceleration would be zero, which has advantages in solving the linearised equations, as well as improvements in efficiency of numerical computations. The linearised solution was developed in stages. Starting with a new elegant form of the Schwarzschild acceleration vector, first order and second order

components were identified. At each point it was demonstrated that the deflection and delay can be easily computed with the new equations, and shown to match known estimates, where such estimates already exist. The clear and straightforward way in which these known results can be replicated (and extended, in one case), demonstrates the versatility of this new method, and suggests that there may be more situations in which this new approach may be useful.

It was shown that inclusion of the second-order rotational components is now a straight-forward matter, following naturally from the linearised Schwarzschild expansion. Again deflection and delay are calculated to second order accuracy, and shown to match known values, as well as generalising an existing formula for calculating delays. The new formulae were used to model delays of pulsar signals past a rotating black hole.

The assumption used in this work, that the effect on a light ray due to multiple massive objects can be approximated by summation of the individual acceleration components is analogous to the same assumption in Newtonian gravity. Testing of this assumption by comparison with numerical solutions of the full Einstein equations would be a fascinating topic for future study. It may also be possible to make some analytical comparisons with solutions that have been proposed for systems of multiple masses, such as the double Kerr solution (Dietz & Hoenselaers, 1985). Chapter 4 of the current study has implicitly assumed that the composition of accelerations is valid to at least second order in the Schwarzschild radius, and it would be of great interest to know whether this is so, both from a practical viewpoint for the use of the techniques presented here, and also informing how valid is such an analogy with Newtonian gravity.

Other topics for future research include more detailed comparison with the thin

lens approach, identifying situations where there is a measurable difference between the two approaches, and thus where the kinematic method may be more useful. Additionally, modelling of light paths through a thicker lens, with comparison to the multi-layer thin-lens approach would be interesting. Finally, modelling of systems where we drop the assumption that the masses are static during the passing of the light ray would be of interest. These suggestions for future study have been kindly suggested by the examiners of this thesis.

The approach presented in this thesis provides a new way to model light paths, including deflection angles and travel time delays, for rays passing near to massive objects. The method has proved versatile and robust, allowing simple and accurate calculations to be made, and providing a new way to produce caustic maps. In this work, the focus has been on micro-lensing, but areas for future study could also include strong lensing models, mapping images at the source plane to distorted versions at the observer's plane. Another subject for study could be to look for efficient ways to model light paths passing near or through more complicated distributions of matter, such as galaxies or clusters of galaxies, using the linearised formulae presented here.

Bibliography

Bartelmann, M. (2010). Gravitational lensing. Classical and Quantum Gravity, 27(23), 233001.

Bennett DP. 2008. Detection of Extrasolar Planets by Gravitational Microlensing. In Exoplanets: Detection, Formation, Properties, Habitability, ed. J Mason, pp. 47–88. Berlin: Springer

Bond, I. A., Udalski, A., Jaroszyński, M., Rattenbury, N. J., Paczyński, B., Soszyński, I., ... & Yock, P. C. M. (2004). OGLE 2003-BLG-235/MOA 2003-BLG-53: a planetary microlensing event. The Astrophysical Journal Letters, 606(2), L155.

Boroson, T. A., & Lauer, T. R. (2009). A candidate sub-parsec supermassive binary black hole system. Nature, 458(7234), 53-55.

Burgay, M., D'Amico, N., Possenti, A., Manchester, R. N., Lyne, A. G., Joshi, B. C., ... & Lorimer, D. R. (2003). An increased estimate of the merger rate of double neutron stars from observations of a highly relativistic system. Nature, 426(6966), 531-533.

Capozziello, S., de Ritis, R., Man'ko, V. I., Marino, A. A., & Marmo, G. (1997). Defocusing gravitational microlensing. Physica Scripta, 56(2), 212.

Carroll, S. M. (2004). Spacetime and geometry. An introduction to general relativity. Addison Wesley, San Francisco.

Chandrasekhar, S. (1983). The mathematical theory of black holes. Clarendon Press/Oxford University Press (International Series of Monographs on Physics. Volume 69).

Dietz, W., & Hoenselaers, C. (1985). Two mass solutions of Einstein's vacuum equations: The double Kerr solution. Annals of Physics, 165(2), 319-383.

Dymnikova, I. G. (1986). Motion of particles and photons in the gravitational field of a rotating body. Soviet Physics Uspekhi, 29(3), 215.

Edery, A., & Godin, J. (2006). Second order Kerr deflection. General Relativity and Gravitation, 38(11), 1715-1722.

Einstein, A. (1936). Lens-like action of a star by the deviation of light in the gravitational field. Science, 84(2188), 506-507.

Ellis, R. S. (2010). Gravitational lensing: a unique probe of dark matter and dark energy. Philosophical Transactions of the Royal Society A: Mathematical, Physical and Engineering Sciences, 368(1914), 967-987.

Fischbach, E., & Freeman, B. S. (1980). Second-order contribution to the gravitational deflection of light. Physical Review D, 22(12), 2950.

Gaudi, B. S. (2012). Microlensing surveys for exoplanets. Annual Review of Astronomy and Astrophysics, 50, 411-453.

Gould, A., & Loeb, A. (1992). Discovering planetary systems through gravitational microlenses. The Astrophysical Journal, 396(1), 104-114.

Jaki, S. L. (1978). Johann Georg von Soldner and the gravitational bending of light, with an English translation of his essay on it published in 1801. Foundations of Physics, 8(11-12), 927-950.

Kenyon, I. R. (1990). General relativity. Oxford University Press.

Laguna, P., & Wolszczan, A. (1997). Pulse arrival times from binary pulsars with rotating black hole companions. The Astrophysical Journal Letters, 486(1), L27.

Mao, S., & Paczyński, B. (1991). Gravitational microlensing by double stars and planetary systems. The Astrophysical Journal, 374, L37-L40.

Mao, S., Kerins, E., & Rattenbury, N. J. (2007). Extrasolar planet detections with gravitational microlensing. Proceedings of the International Astronomical Union, 3(S249), 25-30.

Michell, J. (1784). On the means of discovering the distance, magnitude, &c. of the fixed stars, in consequence of the diminution of the velocity of their light, in case such a diminution should be found to take place in any of them, and such other Data should be procured from observations, as would be farther necessary for that purpose. By the Rev. John Michell, BDFRS In a letter to Henry Cavendish, Esq. FRS and AS. Philosophical Transactions of the Royal Society of London, 74, 35-57.

Misner, C. W., Thorne, K. S., & Wheeler, J. A., (1973). Gravitation. Freeman and Company. San Francisco. (Chapter 23)

Mollerach, S., & Roulet, E. (2002). Gravitational lensing and microlensing. Singapore: World Scientific.

Mortlock, D. J., & Turner, E. L. (2001). Gravitational lensing in modified Newtonian dynamics. Monthly Notices of the Royal Astronomical Society, 327(2), 557-566.

Newton I., (1704), Opticks, Fourth Ed., Reprint 1931, G. Bell and Sons, London

Paczyński B., (1986). Gravitational microlensing by the galactic halo. The Astrophysical Journal, 304, 1-5.

Perkins P., (2006). smoothhist2d. MatLab Central File Exchange, www.mathworks.com.au/matlabcentral/fileexchange/13352-smoothhist2d

Robertson, D. S., Carter, W. E., & Dillinger, W. H. (1991). New measurement of solar gravitational deflection of radio signals using VLBI. Nature, 349(6312), 768-770.

Schneider P., Ehlers J., Falco E., 1992, Gravitational Lenses, Springer-Verlag, New York.

Schneider, P., & Weiss, A. (1986). The two-point-mass lens-Detailed investigation of a special asymmetric gravitational lens. Astronomy and Astrophysics, 164, 237-259.

Shapiro, I. I. (1964). Fourth test of general relativity. Physical Review Letters, 13(26), 789.

Sumi, T., Bennett, D. P., Bond, I. A., Udalski, A., Batista, V., Dominik, M., ... & Pedretti, E. (2010). A cold Neptune-mass planet OGLE-2007-BLG-368Lb: cold Neptunes are common. The Astrophysical Journal, 710(2), 1641.

Treder, H. J., & Jackisch, G. (1981). On Soldner's Value of Newtonian Deflection of Light. Astronomische Nachrichten, 302(6), 275-278.

Walters, S. J., & Forbes, L. K. (2011). A note on a linearized approach to gravitational lensing. Monthly Notices of the Royal Astronomical Society, 416(4), 3067-3074.

Walters, S. J., & Forbes, L. K. (2014). Rotating gravitational lenses: a kinematic approach. Monthly Notices of the Royal Astronomical Society, 444(3), 2470-2486.

Walters, S. J., Forbes, L. K., & Jarvis, P. D. (2010). A kinematical approach to gravitational lensing using new formulae for refractive index and acceleration. Monthly Notices of the Royal Astronomical Society, 409(3), 953-962.

Wambsganss, J. (1997). Discovering Galactic planets by gravitational microlensing: magnification patterns and light curves. Monthly Notices of the Royal Astronomical Society, 284(1), 172-188.

Wambsganss, J. (1998). Gravitational lensing in astronomy. Living Rev. Relativity, 1, 12.

Weinberg, S. (1972). Gravitation and cosmology: Principle and applications of general theory of relativity. John Wiley & Sons.

Witt, H. J., & Mao, S. (1994). Can lensed stars be regarded as pointlike for microlensing by MACHOs?. The Astrophysical Journal, 430, 505-510.

Zabel, S. A., & Peterson, J. B. (2003). Extended source diffraction effects near gravitational lens fold caustics. The Astrophysical Journal, 594(1), 456.